COMPARING THE ACCURACY OF BLUETOOTH LOW ENERGY AND UWB TECHNOLOGY FOR IN-ROOM POSITIONING

A Major Qualifying Project

WORCESTER POLYTECHNIC INSTITUTE

In partial fulfillment of the requirements for the

Degree of Bachelor of Science in Electrical and Computer Engineering

By:

Myo Min Thein

Son Nguyen

Danielle Kennon

Advisor: Professor Kaveh Pahlavan

April 22, 2019

Table of Contents

Executive Summary

The invention of global navigation satellite systems such as the US's Global Positioning System (GPS), Russia's GLONASS, the European Union's Galileo, and China's BDS has allowed unprecedented ease in positioning and navigation (Muller, 2013). However, while these satellite-based radio-navigation systems can accurately locate one's position using distance estimation algorithms, their accuracy is greatly diminished in indoor areas and in locations where satellite signals are obstructed. Therefore, a need exists for systems that can estimate location of personnel and equipment in those enclosed areas which navigation satellite systems cannot reach. Indoor positioning systems that make use of wireless antennas and beacons have recently emerged to address this problem.

While the potential for indoor positioning and navigation beacons is prevalent, the technology is very much in its infancy stage. Beacons that have emerged over the last ten years utilize Bluetooth Low Energy (BLE) technology to locate a user or object by using complex algorithms that estimate the user's distance from a predefined position of a set of beacons. More recently, UWB (UWB) technology has begun to emerge as a positioning alternative. Theoretical research suggests that UWB may have the ability to make distance estimations with even greater accuracy, dominating the traditional BLE positioning model. However, due to their novelty, UWB positioning beacons have yet to join their BLE competitors in the market, and little evidence exists to prove their superiority.

While other subtle variations exist, the most critical difference between BLE and UWB positioning technologies lie in their distance estimating algorithms. BLE technology estimates location using Received Signal Strength (RSS) measurements and distance-based path-loss modelling. The UWB technology estimates the distance based on Time of Arrival (TOA). This change in methodology is rather powerful, eliminating distance-based random variables and simplifying the estimation in a way that should theoretically increase its accuracy.

Our Major Qualifying Project compares the accuracy of UWB and BLE distance estimations for short distance in-room positioning. We gathered data by exploring the ranging of both technologies using commercial BLE beacons and a network analyzer using UWB signals. We then use MATLAB to develop a path-loss model to understand and interpret the BLE's RSS measurements, and process the UWB's TOA measurements. We developed a comparison procedure using Cramer-Rao Lower Bound (CRLB) and discussed the results as they pertain to localization applications in industry. Our final conclusions suggest that UWB is more accurate than BLE technology, with accuracy up to 30cm, compared to BLE within 1m.

Abstract

The purpose of this project is to thoroughly compare the accuracy of UWB and BLE distance estimations in short range in-room application. We gather data with both technologies, and we use algorithms to realize distance estimations with MATLAB. CRLB theory demonstrates that estimations made using UWB are more accurate than those made with BLE, where UWB can correctly locate with centimeter accuracy, while BLE is limited to meter accuracy. Our empirical measurement showed that in practice UWB TOA ranging are much more accurate than BLE RSS ranging

Acknowledgements

We would like to offer special thanks to our Academic Advisor, Kaveh Pahlavan, PhD. for his valuable and constructive suggestions throughout and providing us with an opportunity to grow as both engineers and people.

We would also like to acknowledge Zehua Dong for his assistance with understanding our data collection and processing methodology.

Lastly, we would like to thank Julang Ying for his support in understanding UWB technology.

List of Figures

List of Tables

Authorship

Myo Min Thein	Executive Summary Introduction Background Acknowledgements Methodology Results Conclusion
Son Nguyen	Executive Summary Introduction Background Methodology Results Conclusion
Danielle Kennon	Executive Summary Abstract Acknowledgements Introduction Background Methodology Results

1. Introduction

Our team intends to investigate the accuracy of Ultra-Wideband (UWB) technology for the use of indoor distance estimation applications. To do this, we plan to compare the traditionally used BLE technology using Estimote® BLE Proximity Beacons and the more recently developed UWB technology using SkyCross 222-1137C UWB miniature antennas. Preliminary technical research suggests that the accuracy of UWB distance estimations is greater than those of the traditionally used BLE technology. Our project will ultimately evaluate this assertion by developing a comprehensive empirical testbed and quantitative analysis of the accuracy of UWB and BLE technologies. In this section, we will go over the background & motivation as well as provide the general description of our project. Aside from that, we also include the overall outline of this report in this section.

1.1 Background and Motivations

In-room positioning poses a solution to one of today's most prevalent problems in contemporary internet of things (IoT) system: the lack of accurate indoor positioning. Companies and consumers are continually looking to improve sales or quality of life by streamlining processes and making things more convenient using IoT and automated systems. Actions like finding a new restaurant for the first time, delivering mail to the proper address, or mapping and following shipping routes for products, could all be improved if a personal map could show the location of a user relative to his or her destination. In the 1990's, the introduction of the Global Positioning System (GPS) revolutionized how we navigate by using satellites to provide exactly this type of outdoor-map to consumers across the world (Muller, 2013). Today, navigation technology is advancing even further by making its way *indoors*; a realm unrecognizable by the GPS. And that is the reality that we are dealing with today, most if not all IoT systems primarily cater to a specific indoor area, however this is also the realm where our eye in the sky, satelite navigation systems could not reach. Without accurate geolocation data, IoT systems could operate at maximum efficiency as they could not track to see where the users are or where the subjects that they are supposed to control or monitor are. With the use of recently developed BLE and UWB applications, indoor location tracking through distance estimating is made possible. The potential for innovation with positioning technology is of global proportions and includes applications like automatically tracking the location and movement of products in a warehouse, providing real-time information for shoppers as they browse the shelves at a retailer, or monitoring the movement of medical equipment throughout a hospital. Our BLE versus UWB study will provide necessary insights for the further understanding and development of this market.

1.2 Project Description

In order to compare the accuracy of BLE and UWB, our team developed a procedure to measure and analyze the distance estimation error of both technologies. For BLE RSS measurements, we make use of specilized beacons made by Estimote as our transmitter and our phone as the receiver, Our phone will receive and record the BLE signal transmitted by the beacon and the distance between the phone and the beacon can be derived based on the RSS of the BLE signal that the beacon transmitted to the phone. Furthermore, we created plots of both RSS and TOA versus distance for BLE and UWB respectively. Regarding our UWB measurement method, originally we plan on using commercial grade UWB beacon as well, however due to relatively obscurity nature of UWB systems, we were unable to procure UWB beacons

that are affordable and suitable for this project in a timely manner. And thus we decided to simulate UWB ranging through the use of a VNA graciously provided by the CWINS. To collect measurements, we used an Agilent 8753D Vector Network Analyzer (VNA) and two SkyCross 222-1137C UWB miniature antennas - one as the transmitter, and one as the receiver. The transmitter is configured to transmit over a wide spectrum from 3 GHz to 8GHz with a transmit power of 6 db. The receiver is configured to sweep and receive signal on the same spectrum from 3GHz to 8GHz as well. Once the receiver has received the transmitted signal, all of the multipath signal will be recorded but we will only be making use of the direct path. The delay between when the signal is first sent from the transmitter and when the direct path of signal is reached the receiver is the TOA of the transmitted signal, which is used to derive the distance between the transmitter and receiver based on the formulae in chapter 2. We then compared the results using CRLB theory on variance of distance estimated error (DME), which measures the spread of DME among distance estimations. These results have been compiled to provide a detailed comparison of the accuracy of the two technologies, reference to ranging and location estimating. The comparison is based on our newly developed understanding of RSS-based and TOA-based position modelling and measurement of UWB characteristic of a typical in-room office area. We investigate radio propagation for positioning applications, and evaluate performance based on CRLB.

1.3 Outline of Report

For this report, we first define the purpose, motivation and scope of our project in the introduction section. The second part discusses the technical background and details concerning indoor positioning as well as UWB and BLE technologies. We also highlight the CRLB in that section - the primary performance metric that we will be using to compare UWB and BLE in this project. In the third section, we discuss the methodology behind how we collect and gather RSS and TOA measurement data, as well as processing them for performance comparison purposes. After that, we showcase the results of the project, including several graphs and metrics concerning RSS, TOA, and their associated CRLB. Finally, we summarize the findings of the report in the conclusion section, which explains what we have done and suggests some areas for further work.

2. Overview of Indoor Positioning

Indoor positioning technologies are becoming more and more prevalent as businesses and corporations search for innovative ways to improve customer experience, increase revenue, and drive efficiency in the digital age. Ever since its inception, Bluetooth technology has made its way into various sectors of our daily life, from the phones that we use every day to complex medical devices. On one hand, Bluetooth's prevalence and popularity - as well as its status as the industry standard - makes it the first-choice option when it comes to positioning technology. On the other hand, more primitive technologies that were created with positioning application in mind allegedly offer distinct advantages over Bluetooth in accuracy. One such technology is the UWB technology. Originally conceived for communication applications, the interest and development for UWB was waning over time until it was considered for use in positioning applications. In this section, we will give quick rundown of the main two communications standard, BLE and UWB, that we will comparing. Furthermore, we will also laid out and explain some of the mathematical tools that we will be using in this project, primarily the CRLB and equations that relate ranging to positioning.

2.1 Indoor Positioning in Industry

Big-name brands in retail, entertainment, transportation, and logistics have been deploying the technology to advance sales and visibility. In 2014, Macy's used BLE positioning in over 800 stores to send coupons to customers as they passed by relevant items (Laney, 2015). In that same year, Virgin Atlantic distributed BLE beacons throughout London Heathrow Airport to keep passengers up-to-date on local flight entertainment options, promotions, and currency exchange offers (Laney, 2015). Major League Baseball stadiums across the US have also reaped the benefits of BLE location tracking by giving fans the ability to "check-in" as they arrive and receive push-notifications throughout the game (Laney, 2015). Posit, the first of many logistics companies to interact with BLE Beacons, used the technology for indoor parcel tracking (Apsima, 2014). The market for positioning technology is growing at exceptionally aggressive pace as companies across the globe continue to spot the potential for location-tracking in their respective industries. With a forecasted compound annual growth rate of 91.7% in 2017 (Persistence Market Research, 2017) and its limitless possibilities, a strong understanding of indoor positioning technology will prove beneficial to virtually every company and industry across the globe.

2.2 BLE Technology

A BLE Beacon is essentially an antenna, which communicates by transmitting Bluetooth signal. Unlike customary communication using wired connections, Bluetooth antennas work by using radio waves (iBeacon). iBeacon technology can recognize these transmitted signals unnoticeable to the human eye. As opposed to traditional Bluetooth, iBeacon communicates using BLE, a similar wireless network technology that utilizes less power, and therefore results in lower costs. In fact, BLE can last up to 3 years on just a single coin-cell battery and switching to BLE from Bluetooth can cut costs anywhere from 60%-80% (Locatify, 2017). However, adjustable variables like transmit power and interval of signal transmission may cause battery life to be saved or depleted rapidly. Increasing transmit power will allow a BLE beacon to transmit signal over a larger distance and decreasing its transmission interval with result in greater accuracy. However, both changes will lead to greater power consumption.

2.2.1 Positioning with BLE

In 2013, Apple sparked the beginning of indoor positioning with the unveiling of its revolutionary iBeacon technology (iBeacon Insider). iBeacon communicates with a user's smartphone (iOS and Android devices) by estimating distance between the phone and one of several pre-positioned BLE beacons (iBeacon Insider).

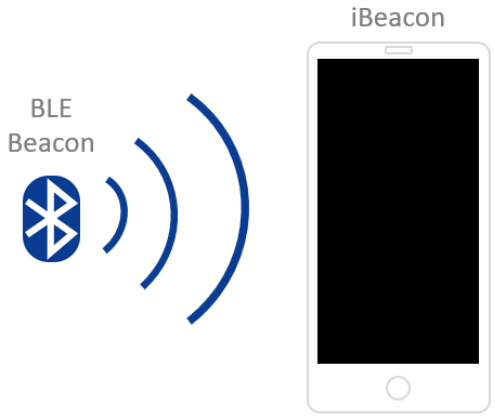

Figure 2.1: A visualization depicting a BLE beacon transmitting to an Apple smartphone using iBeacon. The BLE RSS is then used to derive the distance between the beacon and the smartphone.

These estimations are made in real time through signal transmissions that are unrecognizable to the human eye. Increasing transmit power will allow a BLE beacon to transmit signal over a larger distance and decreasing its transmission interval with result in greater accuracy. However, limitations and dependencies on variable beacon characteristics like transmission power and range greatly affect the life cycle of BLE beacons (Locatify, 2017). Bluetooth positioning applications which require great accuracy usually have a short lifespan due to power consumption, and therefore, are not practical. For this reason, BLE applications are usually *proximity* based, rather than used to determine exact location. The beacons don't necessarily provide an accurate measurement distance, but instead detect whether a signal is present at all (within range). On the contrary, some BLE beacons still aim to provide a measurement of distance between the beacon and the user. These applications estimate distance based on RSS and the principle that signal strength and distance share a mathematical relationship and as one increases, the other decreases (Chen, 2017).

Distance estimations are calculated based on measurements from three different beacons, and geometry is used to find the exact coordinate of the receiver (user). In this case, the relationship between path loss and distance where β_i is the amplitude of the arriving path, I (Pahlavan, 2013):

$$P_d = 10\,log\,[RSS_d] = 10\,log\left[\Sigma_{i=1}^{L}\left|\beta_i^d(t)\right|^2\right] \tag{2.1}$$

2.2.2 Relevant BLE Equipment

There are many companies which offer products and solutions which make use of Bluetooth and BLE technology to implement in-door positioning. Google and Apple each comes up with their own standard, Eddystone and iBeacon respectively, for use in localization and targeted advertisement in large indoor areas. Meanwhile many companies like Estimote also offer beacons that can interact and signals to the user's phone to determine their location (Estimate Inc., 2017). For this particular project, in order to test BLE positioning technology, we choose the BLE location beacon from Estimote. This decision was partly motivated by the fact that previous project group have also used BLE beacons from Estimote and we wanted to compare our results to theirs when we can. Another reason is that, Estimote has extensive experience working with positioning application and they were offering their powerful and accessible software development kit to the public (Estimote Inc., 2017).

Table 2.1: Radio Specifications of Estimote Location Beacon

Identification (Hardware revision)	F3.3
Radio: 2.4 GHz transceiver	Bluetooth® 4.2 LE standard Range: up to 200 meters (650 feet) Output Power: -20 to +4 dBm in 4 dB steps, "Whisper mode" -40 dBm, "Long range mode" +10 dBm Sensitivity: -96 dBm Frequency range: 2400 MHz to 2483.5 MHz No. of channels: 40 Adjacent channel separation: 2 MHz Modulation: GFSK (FHSS) Antenna: PCB Meander, Monopole Antenna Gain: 0 dBi Over-the-air data rate: 1 Mbps (2 Mbps supported)

2.3 UWB Technology

UWB is a communication technology that transmit extremely low-energy signal at low range over a very wide bandwidth at high speed (Pahlavan, 2013). Traditionally, UWB was developed mainly for communication and radar imaging application, however, in recent years, many companies have started developing data collection and positioning applications using UWB (MDPI, 2016).

UWB transmission, unlike conventional spread spectrum transmission, do not interfere with narrowband and modulated carrier wave transmission being transmitted in the same frequency band (MDPI, 2016). UWB radios transmit over a very wide bandwidth, usually at a transmit power of more than 500 MHz, which would allow the spectrum to be shared (MDPI, 2016).

2.3.1 Positioning with UWB

UWB signals are radio waves with very short impulse transmissions, with sharp rises and drops (Pahlavan, 2013). Time travel of UWB signals between two beacons that can be calculated to measure the distance is more accurate than the method of using signal strength of BLE between two beacons. While research suggests UWB may be able to measure the distance with an accuracy of 5 to 10cm, Bluetooth and Wi-Fi can only reach around 5m making the UWB a better positioning technology (MDPI, 2016). However, power consumption of UWB could be a barrier for beacons current design. It uses much less power than Wi-Fi but BLE signals use the least power of all three types. The accuracy of positioning indoor could not be given up since it will use more power than Bluetooth signal. Radio frequency of the signal can be between 3.1 to 10.6 GHz and it is impossible enough to measure the signal strength between two signal waves since transmission can be as low as 100ms each (Pahlavan, 2013). This technology has been expensive in the industry where it is used in robot positioning in warehouse industry but now it is cheap enough to implement on every day's use appliances. Although some smartphone companies are trying to include UWB signal antenna (Elgan, 2013), any of those has been in the market yet. This could be a game changing moment in this IT age for better use of indoor positioning. UWB has five main categories of estimating measurements for positioning that include TOA, angle of arrival, RSS, time difference of arrival, and hybrid (Pahlavan, 2013).

BLE beacons transmit signals exclusively in the 2.4 GHz frequency band, the same band that Wi-Fi signals are transmitted over (Shrestha, 2016). To avoid interference with Wi-Fi signals, BLE signal is transmitted using very little power, which also helps BLE beacon preserve battery life and enables it to operate for a significantly longer time period. Similar to BLE, the UWB signal is also transmitted using relatively little power. The difference, however, is found in UWB's ability to transmit over multiple frequencies, as opposed to BLE's single center frequency. This will allow us to, aside from using the path-loss model, use TOA measurement to locate the user (Pahlavan, 2013).

TOA algorithm works in a way by measuring signal travelling time and multiplying result with speed of light which is 3×10^8 ms^{-1} (Pahlavan, 2013). Indoor positioning using TOA calculation heavily depended on the signal bandwidth. Signal with larger bandwidth allows more accurate ranging (MDPI, 2016). Since UWB systems transmit their signal over multiple frequencies making use of wide bandwidth, it is suitable for indoor positioning through TOA calculation. Simply speaking, the distance from the location of the beacon to that of user can be determined by the following function, with d as the distance, τ

as the TOA and c as speed of light (Pahlavan, 2013). The TOA can be obtained by observing the multipath impulse response and look for the time that the direct path (the first path with the highest amplitude).

$$\boldsymbol{d = \tau \times c} \tag{2.2}$$

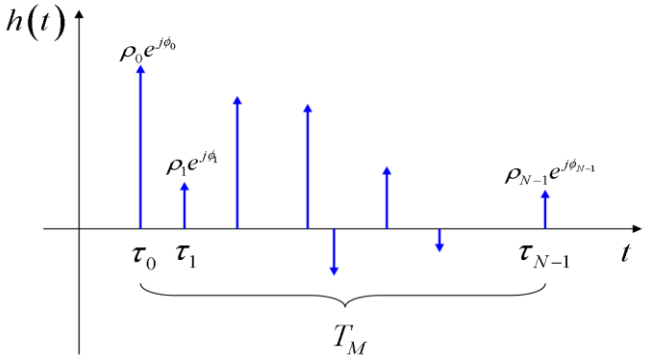

Figure 2.2: Theoretical UWB impulse responses showcasing the effect of multipath path-loss with the x-axis representing the amplitude and y-axis representing the TOA of each path.

Angle of arrival is a method of estimation for signal reception angles from at least two transmitters compared with either signal amplitude or carrier phase across multiple antennas (Pahlavan, 2013). RSS is also used for measuring the distance between beacons and receiver for our project results. It is based on the signal strength that receivers get from the source and estimate the distance using respective path loss formula required for this method. Furthermore, this method can have various error types according to the environment where we are working on such as in a meeting room, stadium, classroom, and so on. When three or more receivers are reading information from a signal source, it can be said as time difference of arrival. However, this situation can be flipped where one or more of the sources are transmitting, and on the other hand, one receiver can determine the location. Hybrid algorithm is for indoor and outdoor positioning purposes where UWB signal receiver and Wi-Fi signal antenna are implemented on the same device so that whenever the user is indoor or outdoor, estimation of location can be tracked. As per our interest in indoor positioning, we will not use hybrid method for this project.

2.3.2 Relevant UWB Equipment

Regarding contemporary UWB-based indoor positioning product and solutions, while it is not as widely supported as BLE-based technology, there are a number of companies that offer UWB-based localization technology. On one hand, companies like Infsoft, Redpoint Positioning and Eliko mainly offer UWB-based indoor positioning for industrial use in manufacturing plants and factories with automation logistic systems. On the other hand, companies like Estimote and Locatify mainly focused on commercial applications such as for navigation assistance and targeted advertisement in large indoor areas. For the purpose of this study, which is to compare the accuracy of BLE-based indoor positioning and that of its UWB counterpart, we looked at various offerings of solutions and products from all the companies mentioned above with the intention of acquiring an evaluation kit from the companies but we were unable to do so due to time as well as budget constraints. Specifically, we found the industrial-focused products to be above our budget while more affordable commercial products are still mostly in research and development state and thus are not available and could not be acquired in time for the completion of this project.

Since the usage of both industrial and commercial grade UWB-based positioning technology is out of the question. We settled on using the virtual network analyzer or VNA, from WPI's CWINS lab to simulate a working UWB-based indoor positioning system. Basically, the two ports of the virtual network analyzer are setup as transmitter and receiver respectively. The transmitter port and the receiver port are both configured to operate and communicate in the frequency band from 3GHz to 8GHz. The virtual network analyzer or VNA itself is then used to capture and record the frequency response and time response in the frequency band from 3GHz to 8GHz. With the time and frequency response capture/measurement obtained from the VNA, we can determine the TOA of the transmitted signal as well as the delay, or the amount of time that it takes for the transmitted signal to reach the receiver starting from the time it was first transmitted. More detail regarding our UWB TOA measurement system will be included in part 3, the methodology section.

2.4 Overview of CRLB for Ranging and Positioning

The CRLB is a statistical theorem which can be used to determine the lower bound on the variance of a possible unbiased estimation model. The theorem uses an estimator's standard deviation to explain the "closest" an estimator will ever be to the actual value. The CRLB is often used to judge the accuracy or capabilities of different estimation models.

2.4.1 CRLB for RSS-based Ranging using BLE Technology

The CRLB theorem can be directly applied to indoor BLE positioning applications to evaluate the accuracy of a path-loss model's predictions. If a certain model for observed power O is strongly dependent on some variable distance d, then the probability density function f(O; d) should be able to estimate O very accurately. In contrast, if O is weakly dependent on d, then f(O; d) will likely not give a very accurate estimate of a O. The general relation between the path-loss and distance in a given environment is modelled by the following equation (Pahlavan, 2013):

$$\boldsymbol{O = P_r = P_0 - 10\alpha log d + X(\sigma_{SF}) = g(r) + X(\sigma_{SF})} \tag{2.3}$$

Where O or P_r is the received power, P_0 is the constant transmitting power, and d is the distance. The variable α is properly named the distance power gradient and describes the relationship between distance and power. X(σ) is the Gaussian distributed random variable that accounts for the effects of shadow fading. Because X(0) is normally distributed with a mean value of 0, the pdf f(0/d) can be calculated as follows (Pahlavan, 2013):

$$\boldsymbol{F = \frac{|g(r)|^2}{\sigma^2}} \tag{2.4}$$

$$f\left(\frac{O[0]}{d}\right) = \frac{1}{\sqrt{2\pi\sigma_{SF}}} \times e^{-\left[\frac{(O-P(d))^2}{2\sigma_{SF}^2}\right]}$$

$$= \frac{1}{\sqrt{2\pi\sigma_{SF}}} \times e^{-\left[\frac{(P_r - P_0 + 10\alpha log d)^2}{2\sigma_{SF}^2}\right]} \quad (2.5)$$

This equation is also known as the Likelihood Function (LF) where LF = f(O; d). To get rid of the exponential, it is often useful to compute to the Log Likelihood Function (LLF) as well, which is simply the natural logarithm of the likelihood function (Pahlavan, 2013):

$$LFF = ln[LF] = ln[f(O[0];\, d)]$$

$$= -ln\sqrt{2\pi\sigma_{SF}^2} - \frac{1}{2\sigma_{SF}^2}(P_r - P_0 + 10\alpha log d)^2 \quad (2.6)$$

Because the likelihood function is an exponential, the accuracy of the estimator is measured by the sharpness of the generated curve. To quantify this value, we can take the second derivative of the function, a procedure which analyzes the curvature of any equation (Pahlavan, 2013):

$$\frac{\partial ln\, f(O/d)}{\partial d} = \frac{1}{\sigma_{SF}^2}(P_r - P_0 - 10\alpha log d)$$

$$\frac{\partial^2 ln\, f(O/d)}{\partial d^2} = \frac{10^2\alpha^2}{(ln\,10)^2\sigma_{SF}^2 d^2} \quad (2.7)$$

In theory, we can say that σ^2 is ultimately equal to the negative reciprocal of the second derivative of the probability density function f(O; d). However, this will only hold true for a specific set of data. In order to generalize, we must consider the expected sharpness of the entire curve by using the expectation of the second derivative over all of O. The CRLB Theorem uses this equation for minimum variance to set a lower bound for the accuracy of a given estimator. The theorem states that as long as pdf, f(O; d) satisfies the regulatory condition where $-E\left[\frac{\partial^2 ln\, p(Y[0];A)}{\partial A^2}\right] = 0 \;\; \forall\, 0$, then the variance of any unbiased positioning estimator must can be calculated by (Pahlavan, 2013):

$$\sigma_P^2 = CRLB = F^{-1} = \frac{(ln\,10)^2\,\sigma_{SF}^2 d^2}{100\,\alpha^2} \quad (2.8)$$

2.4.2 CRLB for TOA-based Positioning using UWB Technology

Similar to BLE applications, the CRLB theorem can be directly applied to indoor TOA positioning applications to evaluate the accuracy of an estimation model based on signal propagation delay. If a certain model for observed power O is strongly dependent on a variable distance d, then the probability density function f(O; d) should be able to estimate O very accurately. In contrast, if O is weakly dependent on d, then f(O; d) will likely not give a very accurate estimate of a O. The general relation between the transmitted pulse s(t) and the observed signal at the receiver in free space is modelled by the following equation [Principles of Wireless Access and positioning (Pahlavan, 2013):

$$\boldsymbol{O}(\boldsymbol{t}) = \boldsymbol{s}(\boldsymbol{t}-\boldsymbol{\tau}) + \boldsymbol{\eta}(\boldsymbol{t}) \tag{2.9}$$

Where η(t) is the additive white Gaussian noise component with a spectral height of $N_0/2$ observed at the receiver. By observing the entire pulse in a Gaussian noise with variance of σ^2, the probability density function can be written as (Pahlavan, 2013):

$$\boldsymbol{f}(\boldsymbol{O}[\boldsymbol{0}];\boldsymbol{\tau}) = \frac{1}{\sqrt{(2\pi\sigma_{SF})^K}} \exp\left\{-\frac{1}{2\sigma_{SF}{}^2}\sum_{k=1}^{k}[\boldsymbol{O}_k - \boldsymbol{s}_k(\boldsymbol{\tau})]^2\right\}|_{k\to\infty}$$

$$exp\frac{1}{N_0}\int_{T_0}^{\cdot}[\boldsymbol{O}(\boldsymbol{t}) - \boldsymbol{s}(\boldsymbol{t}-\boldsymbol{\tau})]^2\,\boldsymbol{dt} \tag{2.10}$$

The second derivative of the natural log is found (similar to how the second derivative is found for BLE), and the Fisher matrix is calculated (Pahlavan, 2013):

$$\boldsymbol{ln}[\boldsymbol{f}(\boldsymbol{O}[\boldsymbol{0}];\boldsymbol{\tau})] = \frac{\boldsymbol{1}}{\boldsymbol{N_0}}\int_{T_0}^{\cdot}[\boldsymbol{O}(\boldsymbol{t}) - \boldsymbol{s}(\boldsymbol{t}-\boldsymbol{\tau})]^2\,\boldsymbol{dt}$$

$$= \frac{\boldsymbol{1}}{\boldsymbol{N_0}}\int_{T_0}^{\cdot}[\boldsymbol{O^2}(\boldsymbol{t}) - \boldsymbol{2O}(\boldsymbol{t})\boldsymbol{s}(\boldsymbol{t}-\boldsymbol{\tau}) + \boldsymbol{s^2}(\boldsymbol{t}-\boldsymbol{\tau})]^2\boldsymbol{dt} \tag{2.11}$$

Because the second derivative of the estimation of $O^2(t)$ with respect to τ is equal to zero, the Fisher matrix for the TOA estimation is given by (Pahlavan, 2013):

$$\boldsymbol{F_\tau} = \boldsymbol{E}\left[\frac{\boldsymbol{d^2}}{\boldsymbol{d\tau^2}}\left\{\ln\left[\boldsymbol{f}\left(\frac{\boldsymbol{O}}{\boldsymbol{\tau}}\right)\right]\right\}\right] = \frac{\boldsymbol{2}}{\boldsymbol{N_0}}\int_{T_0}^{\cdot}\frac{\boldsymbol{d^2}}{\boldsymbol{d\tau^2}}\boldsymbol{E}[\boldsymbol{O}(\boldsymbol{t})\boldsymbol{s}(\boldsymbol{t}-\boldsymbol{\tau})]\boldsymbol{dt}$$

$$= \frac{\boldsymbol{2}}{\boldsymbol{N_0}}\int_{T_0}^{\cdot}\frac{\boldsymbol{d^2}}{\boldsymbol{d\tau^2}}\boldsymbol{s^2}(\boldsymbol{t}-\boldsymbol{\tau})\,\boldsymbol{dt} = -\frac{\boldsymbol{1}}{\boldsymbol{\pi N_0}}\int_{-\infty}^{+\infty}\boldsymbol{\omega^2}|\boldsymbol{S}(\boldsymbol{\omega})|^2\,\boldsymbol{d\omega} \tag{2.12}$$

Therefore, the CRLB becomes (Pahlavan, 2013):

$$\boldsymbol{CRLB} = \boldsymbol{F^{-1}} = \frac{\boldsymbol{\pi N_0}}{\int_{-\infty}^{+\infty} \boldsymbol{\omega^2 |S(\omega)|^2 \, d\omega}} = \frac{\boldsymbol{1}}{\boldsymbol{\rho^2 \beta^2}} \tag{2.13}$$

Where CRLB is the inverse of SNR (signal-to-noise) ratio and normalized bandwidth for the TOA measurements. In the case of using flat spectrum, CRLB can be calculated by deriving the SNR from (Pahlavan, 2013):

$$\boldsymbol{\rho^2} = \frac{\boldsymbol{2E_s}}{\boldsymbol{N_0}} = \boldsymbol{2 \times SNR \times WT_0} \tag{2.14}$$

And theoretical CRLB that is going to be used for this project to compare with the results from can be described as follows (Pahlavan, 2013):

$$\boldsymbol{\sigma_d} = \boldsymbol{c \times \sigma_T} \geq \frac{\boldsymbol{c}}{\boldsymbol{2\Pi}\sqrt{\boldsymbol{2 \times SNR \times W \times T_M \times (f_0^2 + \frac{W}{12})}}} \tag{2.15}$$

CRLB is represented by σ_d, c is the speed of light, SNR, and f_0 is the frequency at which the signal is pulsed.

2.5 From Ranging to Positioning

Methods of how to measure ranging for both BLE and UWB signals are differentiated and explained in the previous sections. In applications for real-life situations, it is optimum to have both ranging and positioning methods for indoor to be applied and used in electronic devices. Ranging can be achieved by having only two devices; one as a transmitter and another as a receiver; on the other hand, positioning must be done with three or more devices where one must be a receiver end and the rest functioning the transmitting part (Pahlavan, 2013). The more devices are used for positioning, the better information about the device's location inside the room or building can be derived based on the algorithms that are developed in the research development stage. Complex mathematical models are used to process received signals and estimate location using a triangulation approach where (Fig 2.3):

$$\vec{\boldsymbol{O}} = \vec{\boldsymbol{G}}(\boldsymbol{x}, \boldsymbol{y}) + \vec{\boldsymbol{\eta}} \tag{2.16}$$

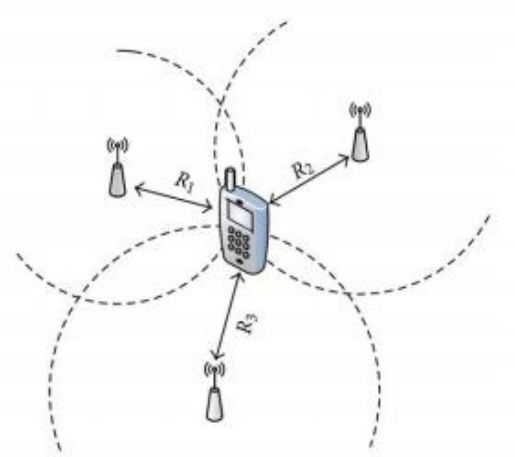

Figure 2.3: Visualization illustrating how a BLE RSS positioning system functions based on the RSS measurement from a smartphone (receiver) that is gathered from signals transmitted from the three BLE beacons

As shown in figure 2.3, difference between ranging and positioning can be clearly identified (Chen, 2017). The arrow between the antenna (transmitter) and phone (receiver) represents the ranging between those two devices whereas communication with two or more transmitters and receiver can be called positioning (Chen, 2017). Complex algorithms that may include taking average of the TOA or RSS based distance measurements are implemented and applied on the devices for use. Based on the purpose of the application and locations such as warehouses, stores, and so on, algorithms for the accuracy of positioning will be differed on the infrastructure of buildings. There are many ways to measure the indoor positioning including TOA and RSS methods. Some of the studies suggest that TOA positioning is not as favorable as RSS although TOA can be reliable for its best accuracy. Indoor location where multipath environments are located make TOA unreliable in taking account into positioning. RSS in this case, although, it does not have perfect accuracy as TOA, it is the best way to measure the positioning for indoor.

2.5.1 RSS Positioning

Measurement method for RSS positioning is similar to the one we discussed in the previous ranging section. From Equation 2.3, the relation between RSS and distances from the receiving points are differed by having N number of different positions instead of one fixed distance between the transmitter and receiver. This equation can be derived as follows: (Pahlavan, 2019)

$$\boldsymbol{P_i = P_0 \; - \; 10\alpha log r_i \; + \; X_i(\sigma)} \tag{2.17}$$

where i stands for the number of receiving points for this positioning in which: (Pahlavan, 2019)

$$\boldsymbol{r_i = \sqrt{(x - x_i)^2 + (y - y_i)^2}} \tag{2.18}$$

Where x and y are actual location of the device and x_i and y_i are locations of the receiving points. Transforming this into classical estimation theory in vector notation with number of RSS observations P = $[P_1\ P_2\ .\ P_N]^T$ in zero mean Gaussian noise X = $[X_1\ X_2\ .\ X_N]^T$: P = G(x, y) + X(σ) where (Pahlavan, 2019)

$$G(x,y) = \begin{bmatrix} P_0 - 10\alpha log\sqrt{(x-x_1)^2 + (y-y_1)^2} \\ P_0 - 10\alpha log\sqrt{(x-x_2)^2 + (y-y_2)^2} \\ . \\ P_0 - 10\alpha log\sqrt{(x-x_N)^2 + (y-y_N)^2} \end{bmatrix} \quad (2.19)$$

These are set of quadratic equations with unknown positions of x and y and each RSS measurement is a range estimate from the transmitters to the device. The location of the device could be anywhere in between these circles as shown in Figure 2.4 and to find the nearest estimate location, localization algorithm must be applied. Using the vector function **G**(x,y) from Equation 2.19, (Pahlavan, 2019)

$$H = \nabla_{x,y}[G(x,y)] = -\frac{10}{ln10}\begin{bmatrix} \frac{x-x_1}{r_1^2} & \frac{y-y_1}{r_1^2} \\ . & . \\ . & . \\ \frac{x-x_N}{r_N^2} & \frac{y-y_N}{r_N^2} \end{bmatrix} \quad (2.20)$$

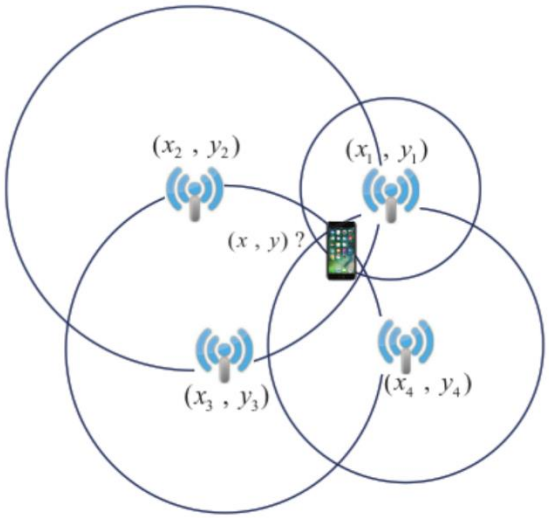

Figure 2.4: Visualization illustrating how a BLE RSS positioning system function based on the RSS measurement that the smartphone, which works as a receiver in this scenario, get from signals transmitted from the four beacons

For this project, we will be focusing on using the CRLB as a bound for the distance estimate accuracy of RSS- based localization algorithm. What makes positioning different from localization is that variance of the shadow fading and distance power gradient are taken into account in estimating the distance. Variations in received power, dP, causes the range estimate to be deviated from getting the reliable estimations. Shadow fading is zero mean Gaussian random variable and covariance of the received power can be formulated as follows: (Pahlavan, 2019)

$$\boldsymbol{E\{|dP|^2\} = cov(dP) = \begin{bmatrix} \sigma^2 & 0 \\ 0 & \sigma^2 \end{bmatrix} = \sigma^2 I} \tag{2.21}$$

Fisher Information Matrix (FIM) for the positioning error caused by shadow fading is given by: (Pahlavan, 2019)

$$\boldsymbol{F = E\{|dr|^2\}^{-1} = \frac{H^T H}{\sigma^2}} \tag{2.22}$$

Then we can calculate the CRLB which is the variance of shadow fading as follows: (Pahlavan, 2019)

$$\boldsymbol{CRLB = \sigma_r^2 = \sigma_x^2 + \sigma_y^2 \geq Tr(F^{-1}) = Tr[\sigma^2 (H^T H)^{-1}]} \tag{2.23}$$

2.5.2 TOA Positioning

Measurement method for TOA positioning is similar to the one we discussed in the previous ranging section. From Equation 2.3, the relation between TOA and distances from the receiving points are differed by having N number of different positions instead of one fixed distance between the transmitter and receiver. This equation can be derived as follows: (Pahlavan, 2019)

$$\boldsymbol{O_i = \tau_i = \frac{r_i}{c} + \eta_{\tau_i}} \tag{2.25}$$

Where x and y are actual location of the device and x_i and y_i are locations of the receiving points. Transforming this into classical estimation theory in vector notation with number of TOA observations $O = [\tau_1 \tau_2 . \tau_N]^T$ in zero mean Gaussian noise $\eta = [\eta_1 \eta_2 . \eta_N]^T$: $O = G(x, y) + \eta$) where: (Pahlavan, 2019)

$$\boldsymbol{G(x,y) = \frac{1}{c}\begin{bmatrix} \sqrt{(x-x_1)^2 + (y-y_1)^2} \\ \sqrt{(x-x_2)^2 + (y-y_2)^2} \\ . \\ \sqrt{(x-x_N)^2 + (y-y_N)^2} \end{bmatrix}} \tag{2.26}$$

These are set of quadratic equations with unknown positions of x and y and each RSS measurement is a range estimate from the transmitters to the device. The location of the device could be anywhere in between these circles as shown in Figure 2.4 and to find the nearest estimate location, localization algorithm must be applied. From Eq 2.26, we can put into vector format given by following: (Pahlavan, 2019)

$$\boldsymbol{H = \nabla_{x,y}\tau = \frac{1}{c}\begin{bmatrix} \frac{x-x_1}{r_1} & \frac{y-y_1}{r_1} \\ . & . \\ . & . \\ \frac{x-x_N}{r_N} & \frac{y-y_N}{r_N} \end{bmatrix}} \tag{2.27}$$

For this project, we will be focusing on using the CRLB as a bound for the distance estimate accuracy of TOA - based localization algorithm. We assume that signal noise ratios of the received signals are the same and FIM for TOA method is the same as we indicated in BLE as below: (Pahlavan, 2019)

$$\boldsymbol{F = E\{|dr|^2\}^{-1} = \frac{H^T H}{\sigma_\tau^2}} \tag{2.28}$$

Then we can calculate the CRLB which is the variance of thermal noise as follows: (Pahlavan, 2019)

$$\boldsymbol{CRLB \geq Tr\left(F^{-1}\right) == \sigma_r^2 = \sigma_x^2 + \sigma_y^2} \tag{2.29}$$

Unlike the RSS positioning measurement noise that is caused by the shadow fading, TOA-based positioning measurement noise is caused by thermal noise. In comparison, thermal noise is so small that distance estimations based on this method becomes more accurate than shadow fading noise.

3. Measurement and Modeling of RSS and TOA

The following section describes the procedures used to collect the data necessary to develop and evaluate distance based on RSS and TOA measurements. LOS (Line of Sight) RSS measurements were taken at various distances in a mid-sized empty room, using Estimote® Location Beacons. LOS TOA measurements were taken in the same room using a network analyzer and two miniature UWB antennas. Data from both procedures was processed using MATLAB. To be more specific, we will be detailing how we take our BLE RSS and UWB TOA measurements. Furthermore, since we devised our own UWB TOA Measuring System as we could not procure UWB beacon in time for the project, we will also be detailing the setup and specifications of our UWB TOA Measuring System in hope that later groups who take on the mantle of responsibility to continue this project in our stead could make use of the groundwork that we have laid.

3.1 Measuring RSS versus Distance using BLE

RSS measurements were taken in a sizeable empty room (AK 206). A room of this size was selected because it closely resembled the size of the room that Estimote® used to advertise/demo its Location Beacons. An empty room was chosen to eliminate the possibility of furniture affecting signal transmission. The Estimote® Location Beacon was placed on a stool at about chest-level. We decided against placing the beacon on the floor to avoid signal refraction. We then used a tape measure to mark various distances on the floor that ranged from 1m-5m away from the beacon. After the floor was marked, we removed the tape measure and stood at the 1m mark. We used an android smartphone (receiver) to communicate with the beacon (transmitter) and read RSS measurements on the smartphone screen, directly facing the beacon. We took about 20 measurements at 1m mark. We followed by taking about 20 measurements with the same procedure and equipment at the 2m mark. We continued taking measurements at each location till we reached to the maximum distance of 5m. All RSS measurements can be found in Table 3, in Appendix B of this document. To evaluate the performance of RSS-based positioning, we used path-loss modelling and the CRLB to find the variance in position estimations using the CRLB *Equation 2.7*.

3.2 Measuring TOA versus Distance using UWB

TOA measurements were taken in the same room (AK 206), under the same conditions, LOS and OLOS as the BLE measurements. Again, the room was intentionally left empty to eliminate any interference or wave-guiding that may be caused by furniture. To collect measurements, we used an Agilent 8753D Vector Network Analyzer (VNA) and two SkyCross 222-1137C UWB miniature antennas - one as the transmitter, and one as the receiver. The transmitter is configured to transmit over a wide spectrum from 3 GHz to 8GHz with a transmit power of 6 db. The receiver is configured to sweep and receive signal on the same spectrum from 3GHz to 8GHz as well. Once the receiver has received the transmitted signal, all of the multipath signal will be recorded but we will only be making use of the direct path. The delay between when the signal is first sent from the transmitter and when the direct path of signal is reached the receiver is the TOA of the transmitted signal, which is used to derive the distance between the transmitter and receiver based on the formulae in chapter 2.

Before starting, we made sure to calibrate the network analyzer by joining transmitter and receiver cables together and lying flat on the floor. We used the VNA's calibration wizard, then detached the cables from each other and attached them to the UWB antennas. Next, we transformed the signal to visually check

that a distance-based time delay was present. An example plot can be seen below in Figure 3.1, where the TOA is recorded on the x-axis.

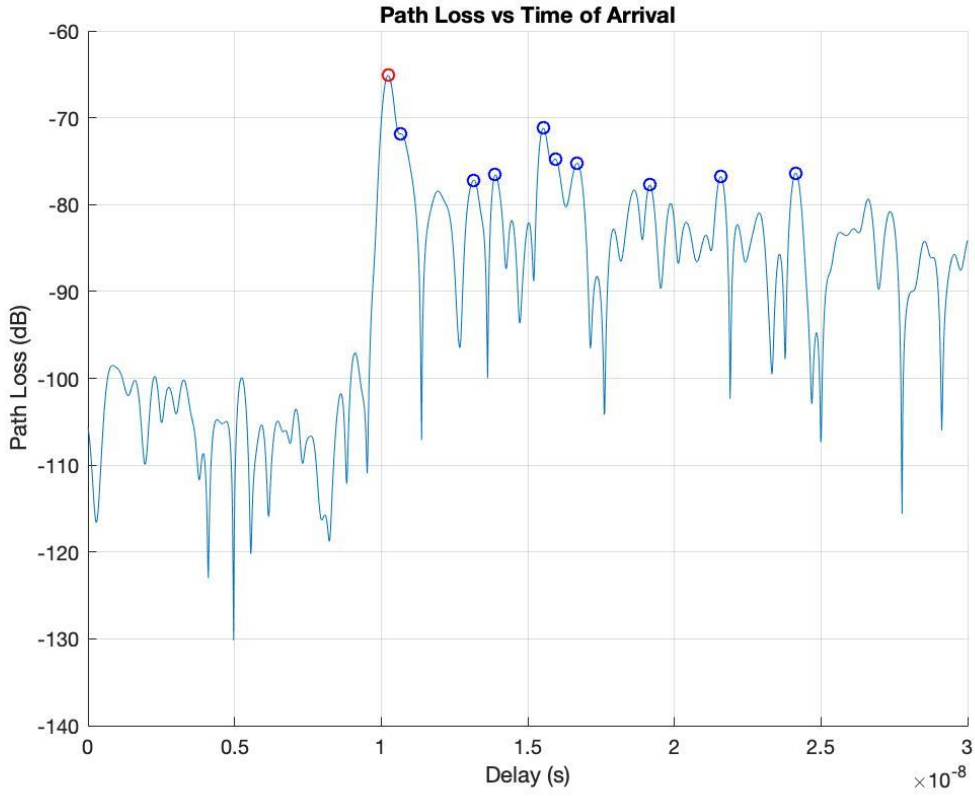

Figure 3.1: Path loss (logarithmic scale) versus delay graph of transformed UWB signal captured using VNA (1m)

It is worth noting that it was much easier to detect the first path's peak using the linear scale as the first path's power is clearly shown to be much higher than that of the other paths whereas in the logarithmic scale the difference is mitigated. Below is the linear version of the same sample shown in Figure 3.2. Details regarding our peak detection method is described further below.

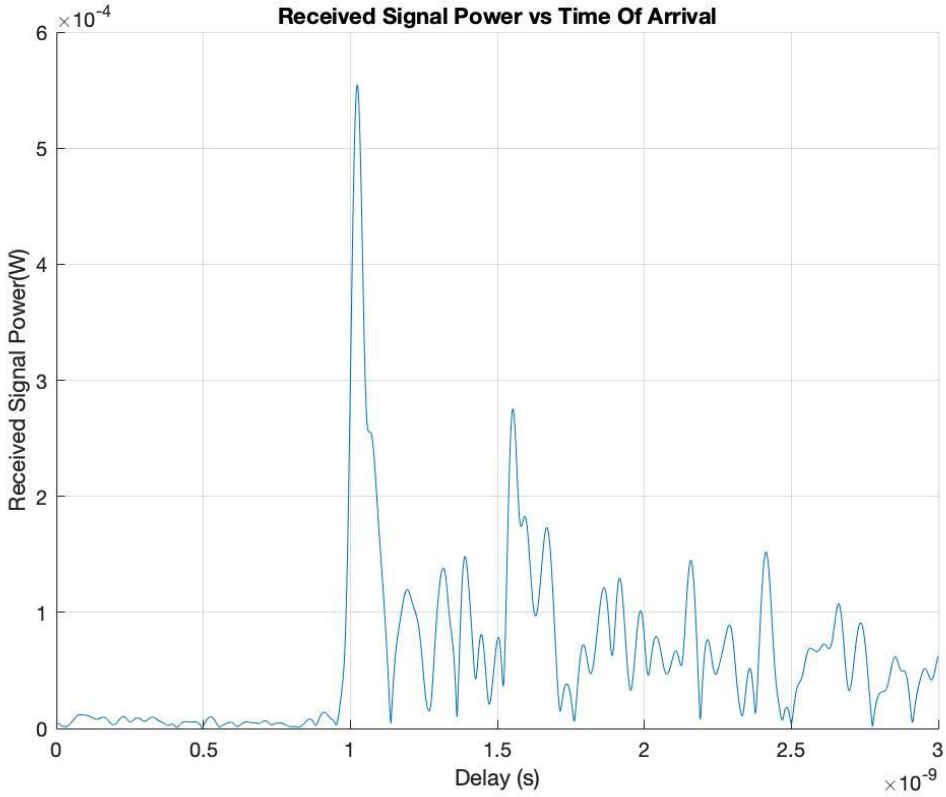

Figure 3.2: RSS (linear) versus delay graph of transformed UWB signal captured using VNA (1m)

After we verify that the antennas were functioning properly, we placed the UWB transmitter on a tripod stand at about chest-level in the corner of the room. We used the tape measure to mark incremental distances on the floor ranging from 10cm - 5m away from the transmitter. Then, we removed the tape measure, and stood at the 10cm mark, holding the receiving antenna. While facing the antennas directly towards each other, we saved the TOA measurement as a ".s1p" file using a USB memory stick. This file format was chosen because we knew we would be able to interpret and process it later with MATLAB. We followed by repeating the same procedure and saving the measurements in the same format at every increment of 10cm until we reached 5m. To evaluate the performance of TOA-based positioning, we used the CRLB to find the variance in position estimations using the CRLB equation, *Equation 2.14*.

3.3 UWB TOA Measuring System

Figure 3.3: Close-up photographs of the Agilent 8753D virtual network analyzer (VNA) and two SkyCross 222-1137C UWB miniature antennas

For gathering the TOA Delay for the UWB ranging part, we make use of the Agilent 8753D Vector Network Analyzer (VNA) and two SkyCross 222-1137C UWB miniature antennas - one as the transmitter, and one as the receiver. Each of the antenna is connected to one of the channels on the Network Analyzer. The antenna's horizontal and vertical positions are secured by the tripods prior to measurement and data gathering. The distance between the antennas themselves are adjusted manually between each data measuring run. We measured TOA delay from distances of 1 m up to 5 m with step size of 0.1 m. To do this, we used a measuring tape to mark various distances across the floor, and to find the exact dimensions of the room as well. The location chosen for the measurement runs is AK 206, an approximately 5.7m by 5.7m room where furniture can be easily moved for the purpose of the experiment.

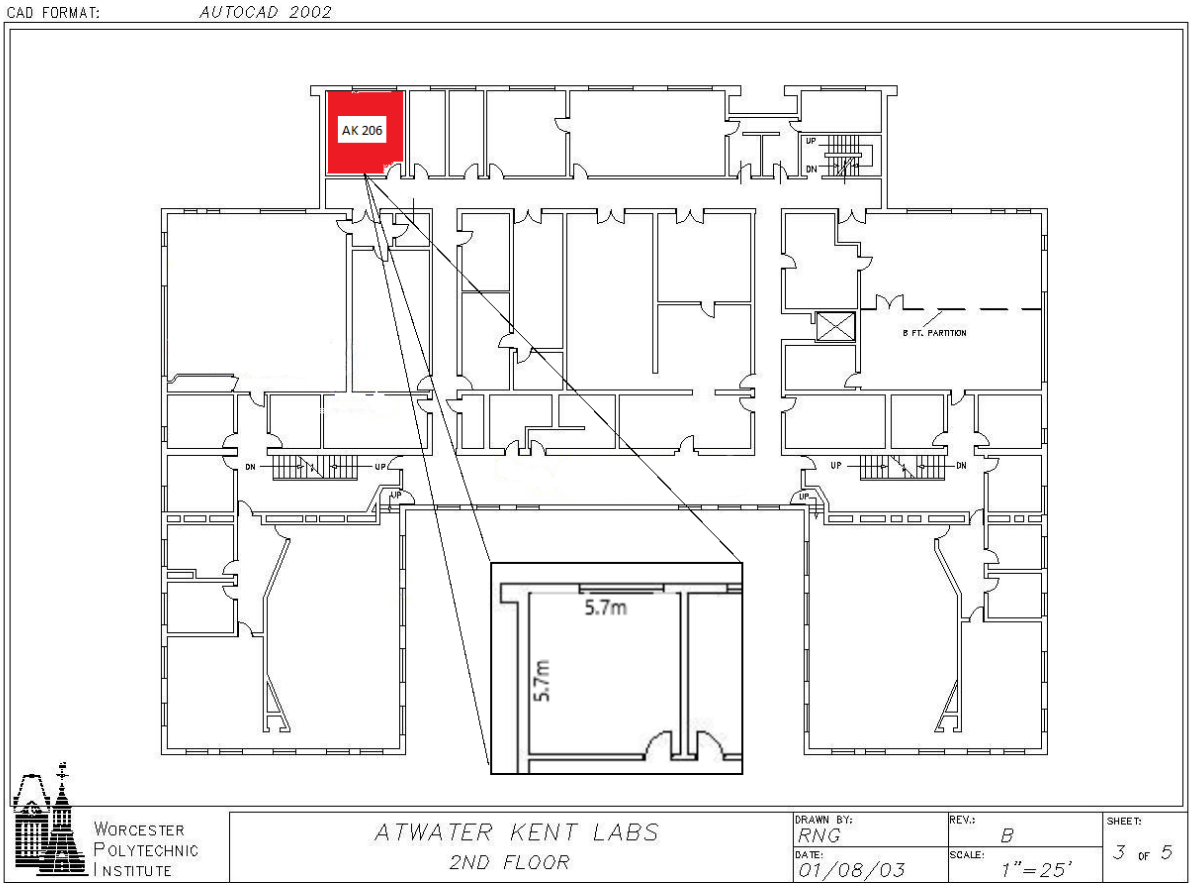

Figure 3.4: Atwater Kent building floor plan, highlighting room ak206 in the top right corner and providing room dimensions in the expanded view at bottom center

After the room was appropriately set up for data collection, we began by calibrating the VNA. In order to see and measure TOA delay using the Network Analyzer, special care must be taken to follow the right steps in a strict calibrating procedure. First, we have to wait up to 30 minutes for the Network Analyzer to start up. Then we must connect the two channels of the analyzer together. It is worth noting that in this step we must make sure that we are connecting the two cables of the two channels while they are on the ground to reduce noises. After that, we must navigate the Sweep options and set the "number of points" option. The recommended settings, 1601, seems to be a reasonable option since it is a sufficient amount of points to see changes in the spectrum, but it is not numerous enough to slow down our operation. The next thing to do is then to set the trace option to "Measure S21". Finally, we can now go to the calibration options and configure them to start the calibration. For this part, it is mostly just shifting through the default options and making sure each one is selected. Finally, the VNA will calibrate automatically, and then the antennas can be attached to the cables so that data collection can begin. Special care must be taken in this step as the lead of the cable are vulnerable to electrostatic discharge so it should not make contact with any parts of our bodies unless it is covered in tin foil first. After the cables have been carefully disconnected, all we have to do next is to connect the antennas to each of the cable which in turn is connected to each of the two channels of the network analyzer.

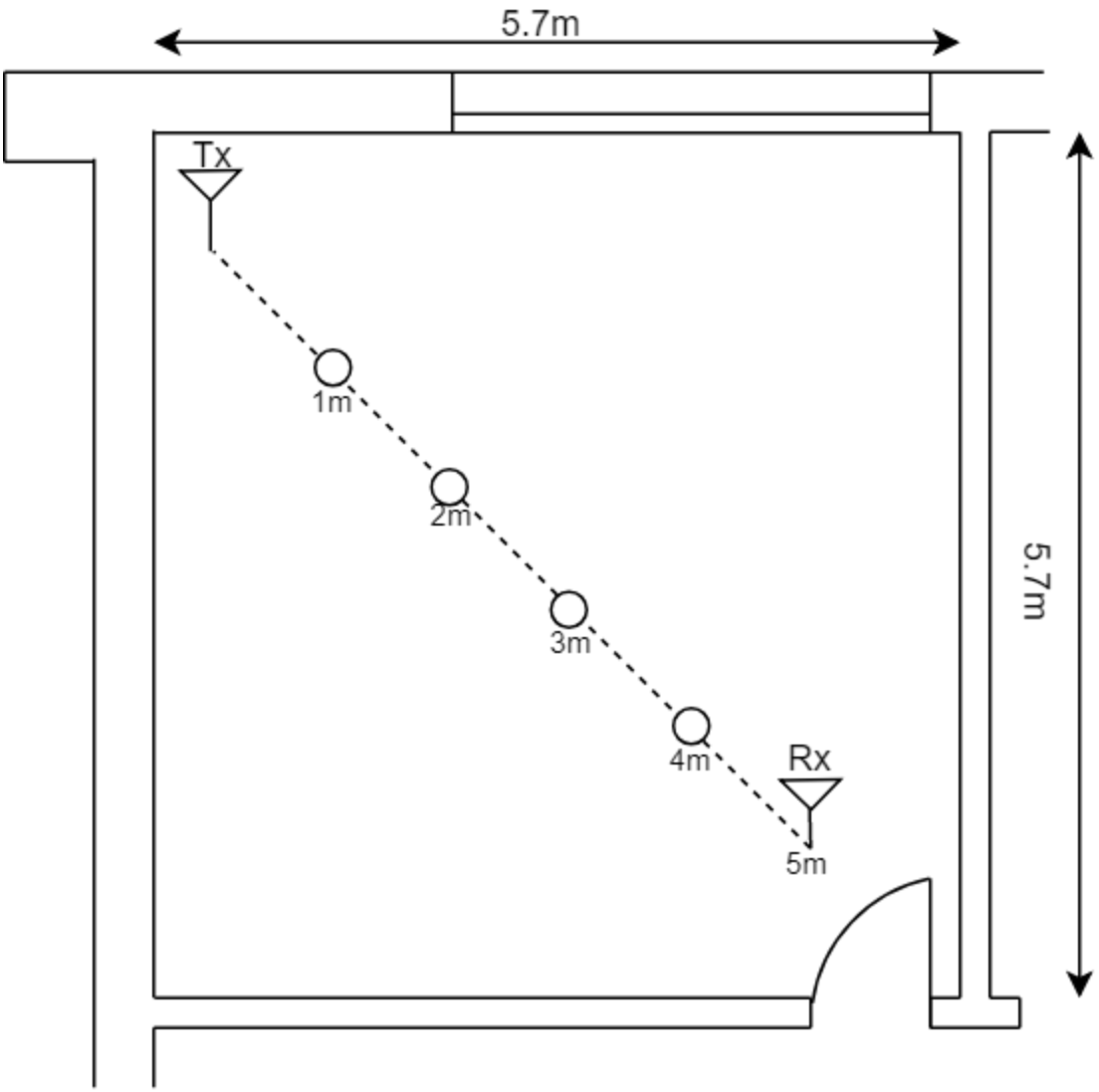

Figure 3.5: UWB and BLE measurement scenarios in room AK 206 with Tx located in the upper right corner of the room while the Rx is moved around between the 1m, 2m, 3m, 4m and 5m mark with 10 measurement taken at each mark

After the set-up was complete, we began our data collection. The transmitting antenna was attached to a tripod and the receiving antenna was held in hand, at the equivalent height. One of us stood, holding the receiving UWB antenna, at the first distance increment (1m), and recorded the received signal and time delay. This was repeated at every distance increment up to 5m.

Apart from measuring LOS for TOA of UWB, we also measured how the signal would be affected in Obstructed Line of Sight (OLOS) conditions. This was done because it more closely models what a user might see when using beacons for ranging or positioning in industry, and during ranging for positioning.

We used our bodies as an obstruction and stood between the signal transmitter and receiver. To analyze the effect, we took measurements at each of the meter up to 5m unlike previous method of incrementing 0.1m from 0 to 5m. However, we put our body as a medium or obstruction and turn around our body 360^0 and take eight measurements at each 45^0 angles for every meter. After that, we followed the procedure as we did on the LOS trials.

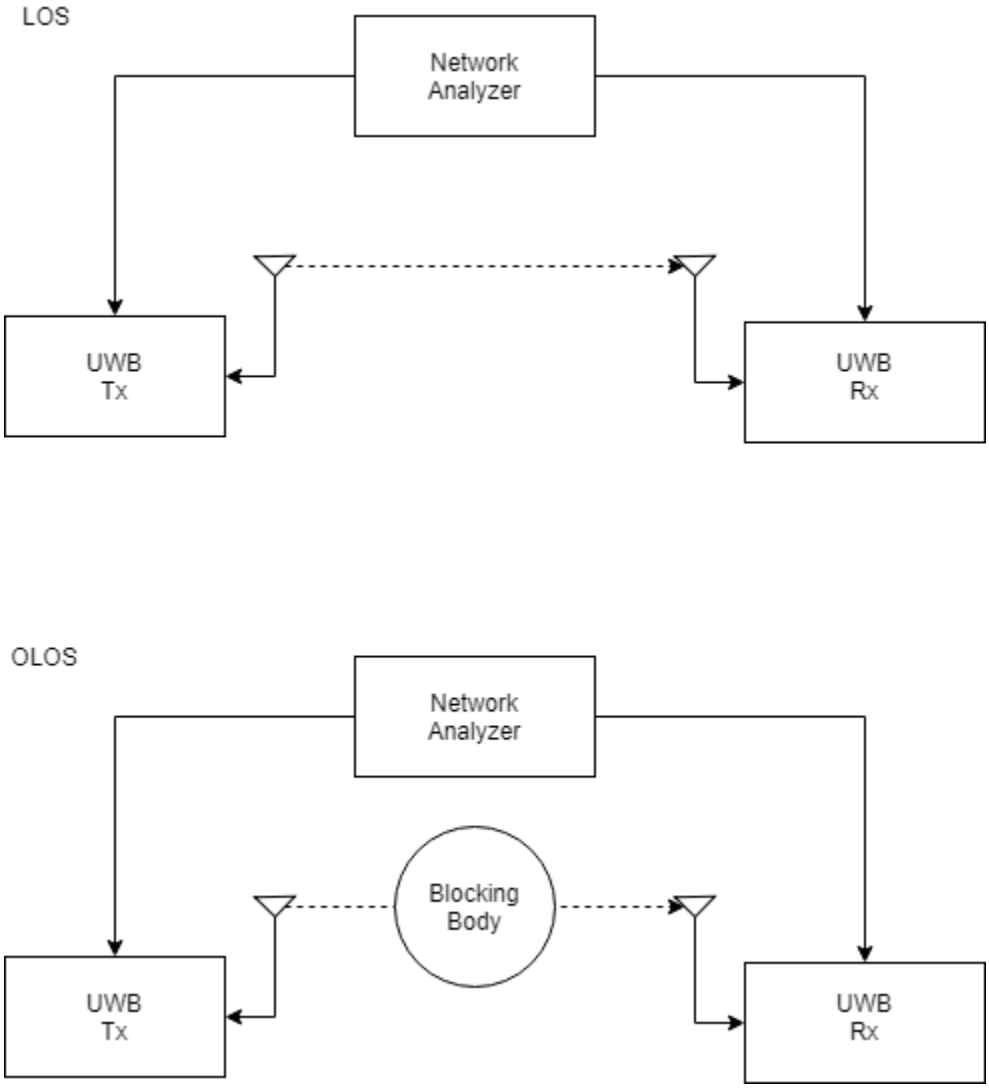

Figure 3.6: LOS & OLOS UWB measurement scenarios with a human body used the blocking body for the OLOS case

While collecting, we can toggle off the transform option so that the Network Analyzer display the frequency spectrum measurement and then navigate to the save file option to save our measurement data to a suitable location. The data will be saved in a "s1p" file format. The s1p files can then be processed by the MATLAB code, which is in our appendix section. A sample measurement, which describes the Time Delay in seconds, has been included in the Appendix as well.

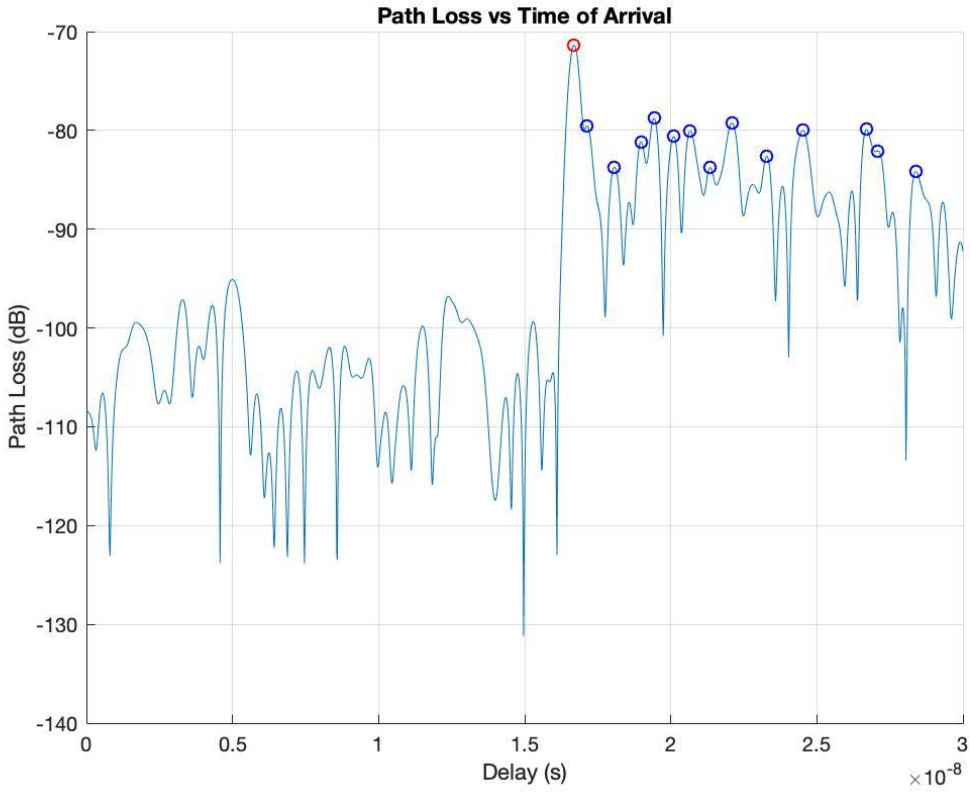

Figure 3.7: Path loss (logarithmic scale) versus delay graph of transformed UWB signal captured using VNA (5m)

Regarding our peak detection method, for the logarithmic representation of the RSS, we need to identify the noise threshold as well as side lobe amplitude for the window function. The peak detection algorithm that we used basically discard the samples that have power level lower than the noise threshold and compared the remaining samples to find the one with the highest RSS. The peak detection function that we used for this project can be found in the appendix.

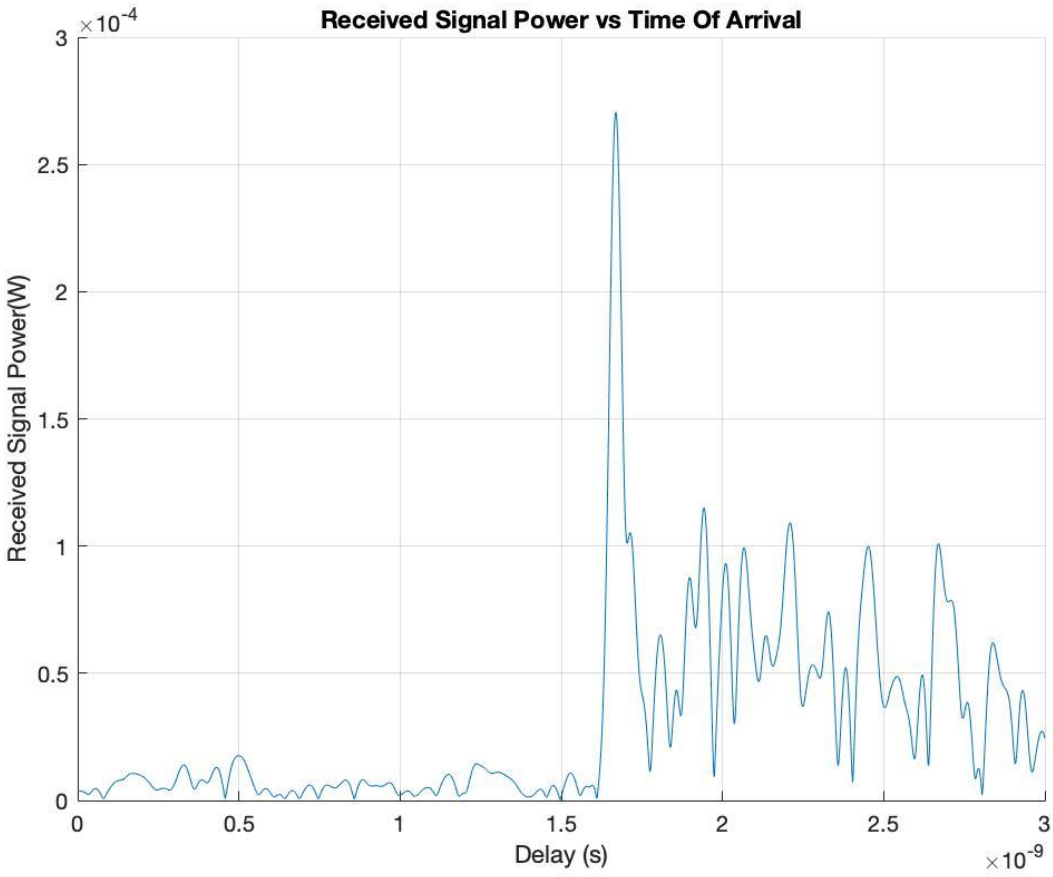

Figure 3.8: RSS (linear scale) versus delay graph of transformed UWB signal captured using VNA (5m)

Generally, the peak detection algorithm that we used for the logarithmic representation of the RSS/path loss wa

s adequate for most of the scenarios that we tested in this project. However, for cases in which the effect of shadow fading is maximized as the blocking body completely blocked the direct path between the receiver and transmitter, the linear representation of the RSS for peak detection. Linear peak detection function nearly identically to its logarithmic counterpart. The only difference is that the noise threshold is used to narrow down time intervals that the first path peak might be situated before the samples in the selected interval are compared to find the peak.

4. Results and Discussion

The following section explains the results of our project. Overall, the results section can be divided into three main subsections: LOS Ranging Results, OLOS Ranging Results and Positioning Results. The LOS and OLOS Ranging Results subsections can be further divided into BLE and UWB results respectively. For the BLE Ranging Results, we have produced graphs depicting RSS versus distance, graphs displaying actual distance versus measured distance, and graphs showing the ranging error versus distance in both LOS and OLOS condition. As for the UWB Ranging Results, we have produced graphs displaying the direct path's path loss versus the distance derived from TOA, actual distance versus distance derived from TOA, distance error versus actual distance, as well as histograms to help visualize the quantity and distribution of the distance error for both LOS and OLOS conditions. The Positioning Results section display the contour of positioning error heat maps in LOS and OLOS condition for both BLE and UWB. The CDF graph of positioning error in LOS and OLOS condition for both BLE and UWB are also included in the Positioning Results section. Finally, we also included positioning error contour heat map as well as CDF graph comparing theoretical CRLB and empirical results for UWB to highlight the difference between theoretical results and what we can get in reality.

4.1 LOS Ranging Results

In this subsection, we display the results for both BLE and UWB ranging in LOS condition. For the BLE results, we have graphs depicting RSS versus distance, graphs displaying actual distance versus measured distance, and graphs showing the ranging error versus distance specifically in LOS condition. For the UWB results, we have graphs displaying the direct path's path loss versus the distance derived from TOA, actual distance versus distance derived from TOA, distance error versus actual distance, as well as histograms to help visualize the quantity and distribution of the distance error. Overall, we can see that even in LOS condition, BLE ranging accuracy are rather poor especially compared to that of UWB

4.1.1 BLE Ranging in LOS

The data collected during our BLE ranging study in LOS has been summarized in a scatter plot below (Figure 4.1). Each received signal is represented by a dot on the graph that describes its magnitude in dB and its measured distance from the transmitting antenna. A line-of-best-fit has been included to illustrate the trend in signal strength as a result of increasing distance. Refer to Appendix B for the full collection of data for the BLE LOS trial.

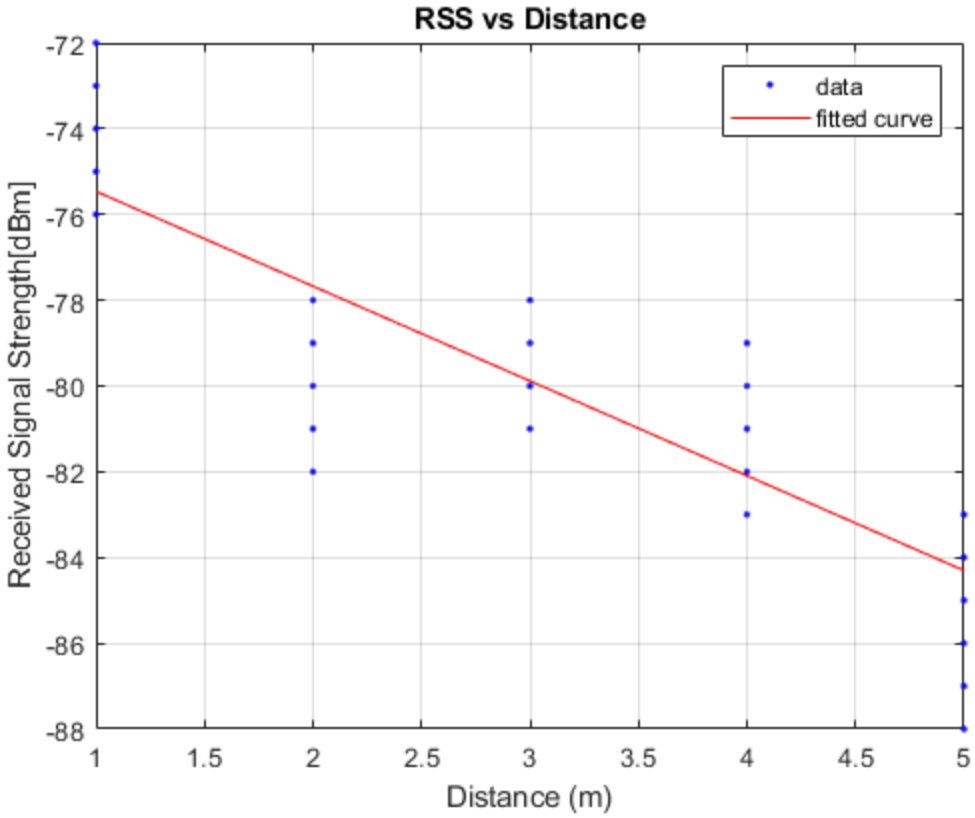

Figure 4.1: RSS versus distance in LOS condition and the best fit line for path-loss modeling for BLE ranging

The trend line suggests that RSS and distance share an inverse relationship, and that RSS decreases as distance increases. The relationship can be quantized by using the line of best fit where:

$$F(x) = -2.211x - 73.25$$

As discussed, this equation describes the relationship between RSS and distance. Recall Eq. 2.3 and notice that the distance power gradient (α) was realized to be 2.211. This is typical of published in-room BLE ranging studies, which suggest that an enclosed empty room usually yields an alpha value of about 2.2 (Pahlavan, 2013).

With this in mind, Eq. 2.3 can be used to estimate the exact distance between the receiving and transmitting BLE antennas. To better understand these estimations, the error of all measurements taken at each distance was determined and summarized in the figure below (Figure 4.2).

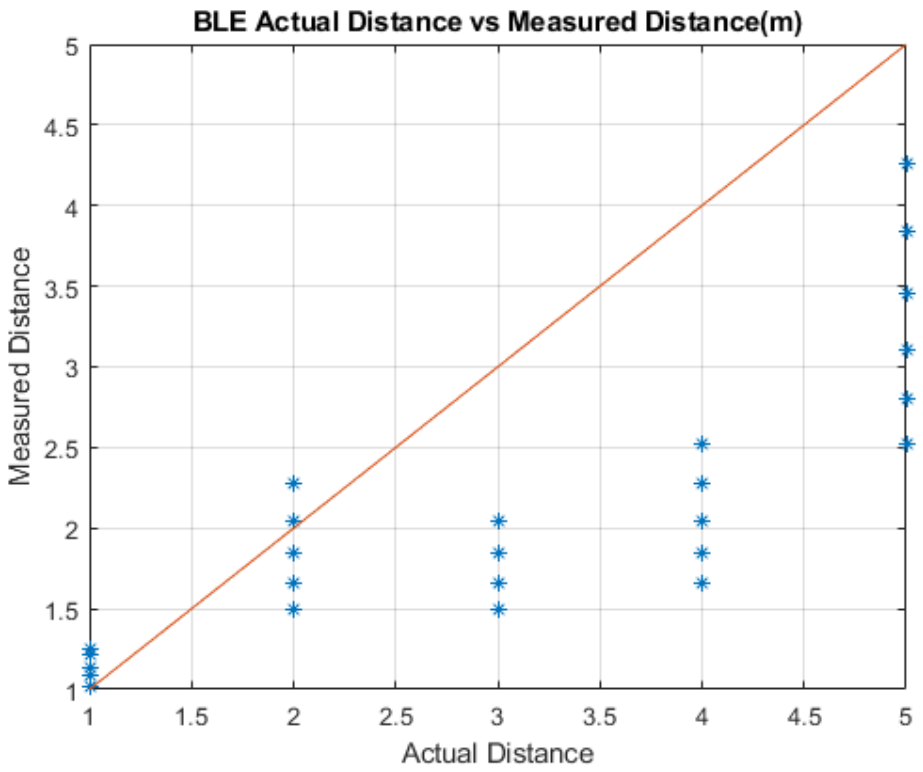

Figure 4.2: Actual distance versus measured distance in LOS condition for BLE RSS ranging with the line represent the ideal distance measurement

Observing the data as represented above, it becomes clear that the error associated with distance estimations is directly related to the physical distance between the receiving and transmitting antennas. The spread of data points at each distance increment indicates the accuracy of the distance estimations. As the spread of the data points (the range of distances) increases, the accuracy of the measurement decreases. It should be noticed that the data points are clustered closest together at the shortest distance, and farthest apart at the longest distance. This change in spread, along with the depicted trend line supports the idea that as distance increases, the spread – and therefore, accuracy of distance estimations, decreases.

As discussed in Chapter 2.4.2, this change in error and accuracy can be fully quantified by using CRLB theory. In this context, the average error at each distance was considered, and the standard deviations of those errors were used to depict the CRLB (Figure 4.3).

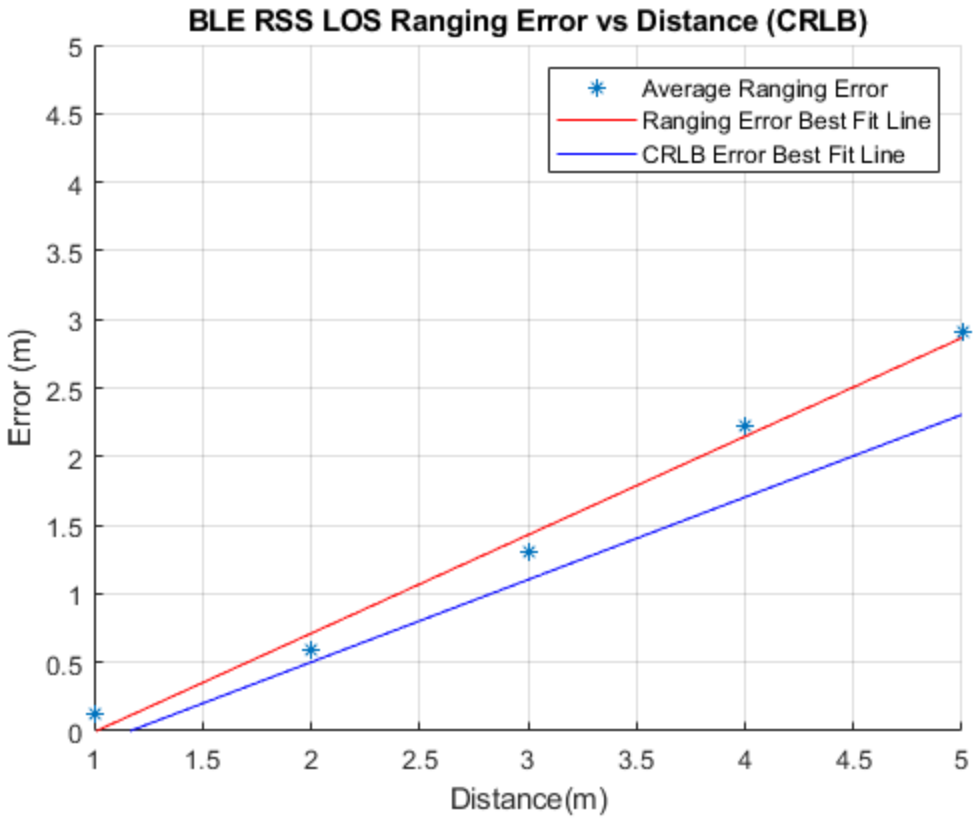

Figure 4.3: Ranging error versus distance in LOS condition for BLE ranging with the asterisks representing the average ranging error at a given distance while the two lines are the empirical and theoretical CRLB best fit curve respectively

The data points depict the standard deviation of the distance estimations made at each location. The red line shows the general trend of those standard deviations, and its positive slope suggests that the standard deviation of error increases as distance between the transmitting and receiving antennas increases.

Using MATLAB and Eq. 2.3, the CRLB was calculated using this data and is depicted by the blue line on the graph. The CRLB considers the best-case scenario, where shadow fading effects are minimized. Through its derivation, the equation for CRLB actually ignores this variable, and identifies the lower bound on the accuracy of distance estimations. This means, that the best accuracy our distance estimation methodology can possibly achieve, (meaning no shadow fading) is essentially the CRLB. The standard deviation of error, which maps accuracy with the consideration of shadow fading, represents the accuracy bound we should really expect.

In this case, the CRLB is dependent on the distance, which can be assumed because it changes as distance changes. At the closest distance of 1m, the CRLB was calculated to be about (0.0709m), and at the farthest distance, the CRLB was found to be (1.7721m). This means that the *best* performance we can expect from our BLE distance estimation methodology can only be correct within 0.0709m of the actual measured distance when the transmitting and receiving antennas are 1m apart. Likewise, the *best* performance we can expect when the transmitting and receiving antennas are 5m apart can only be correct within 1.7721m of the actual measured distance.

The LOS BLE methodology explains that both the accuracy of distance estimations in an enclosed meeting room environment are dependent on the ranging distance between the transmitting and receiving antennas.

4.1.2 UWB Ranging in LOS

The entirety of the data collected during our TOA versus Distance LOS procedure has been depicted in the plot below (Figure 4.4). The waveforms depict the received signal that was observed at various different distances. Unlike the data represented on the BLE graph where the transmission power was a constant 2.4GHz, the TOA methodology involved sweeping the transmission frequency from 3GHz to 8GHz. For this reason, each signal is represented by a waveform rather than a data point.

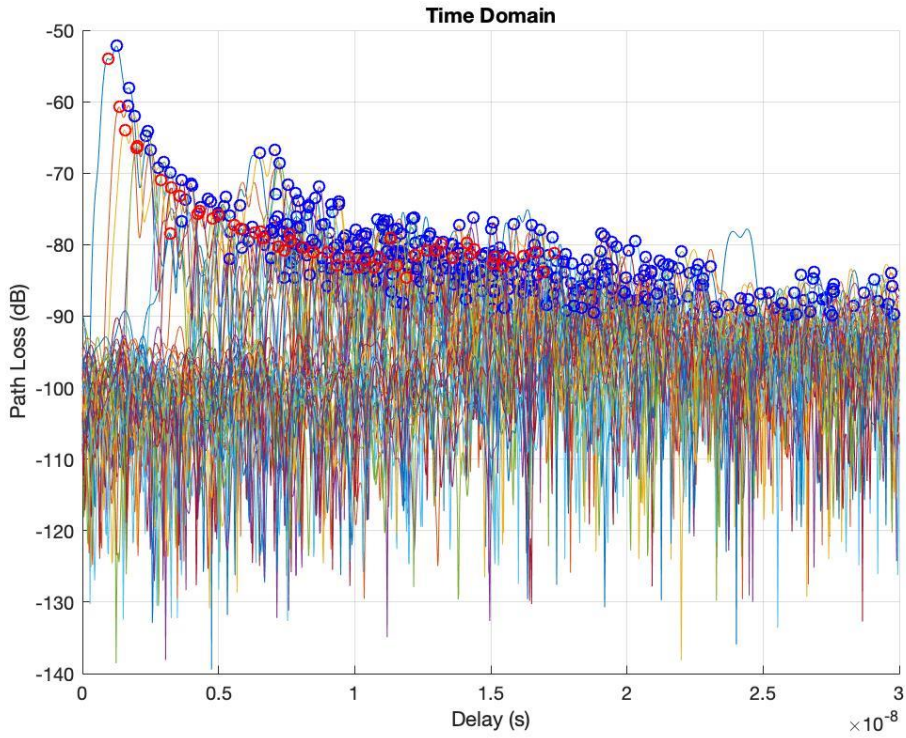

Figure 4.4: Path loss versus delay in seconds for UWB TOA ranging in LOS condition depicting all the data collected during one run of 50 measurements

The peaks of the waveforms, which are the data points which we are interested in, have been marked with circles to clearly identify the path loss and time delay, where red represents the first peak of the waveform and blue represents any subsequent peaks. For the purposes of our project, we are only considering the first peaks (red circles) because we are primarily concerned with first-path path loss of UWB signal.

For clarity and understanding, an additional plot which provides only the first-path path loss of those waveforms was considered and, the Eq. 2.8 was used to produce a graph which depicts TOA first-path path loss versus distance (Figure 4.5).

Recall from Eq. 2.2 that the relationship between TOA and UWB distance estimations can be described by $d = \tau \times c$. The TOA data points gathered from the waveforms are representative of τ. By simply multiplying each point by the speed of light, c, we can depict the relationship between distance and TOA path loss.

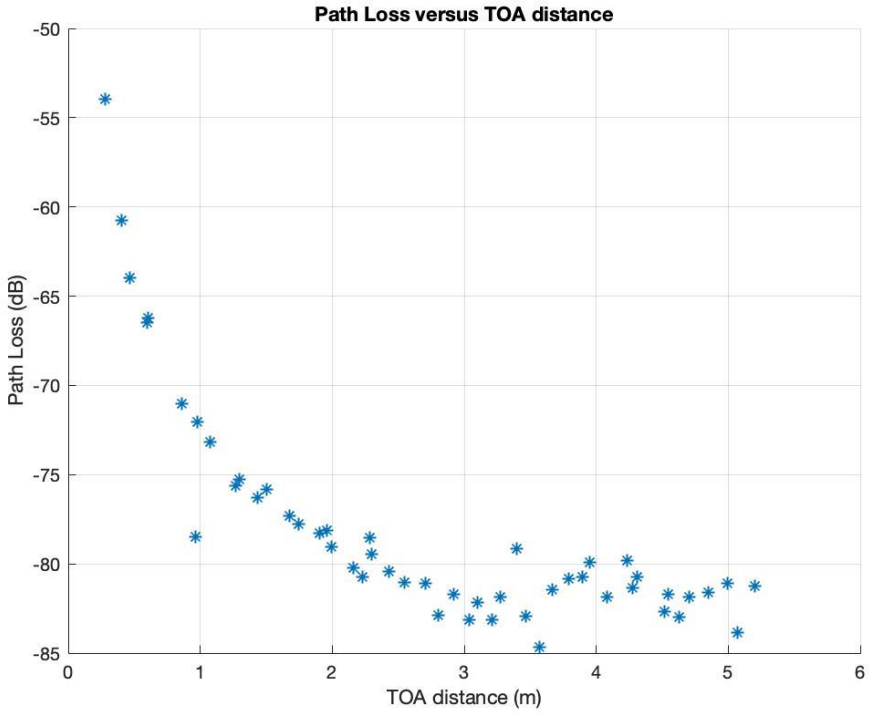

Figure 4.5: Path loss of the direct path versus distance derived from TOA of the direct path for UWB TOA ranging in LOS condition

Our data suggests that a relationship between TOA and Signal Strength in which they are proportional. The curve illustrates that the magnitude of path loss increased as the distance between the transmitting and receiving antennas increased. This is supported by Eq. 2.8, which describes the theoretical relationship between observed power at the transmitting antenna, O(t), and the TOA, τ.

After verifying our data, we assessed its accuracy for distance estimating. We created a graph which depicts the estimated distance using TOA, versus the actual measured distance. Ideally, this curve should be represented as a straight line with a slope of 1, which suggests that the distance estimated by TOA is always equal to the actual measured distance (Figure 4.6).

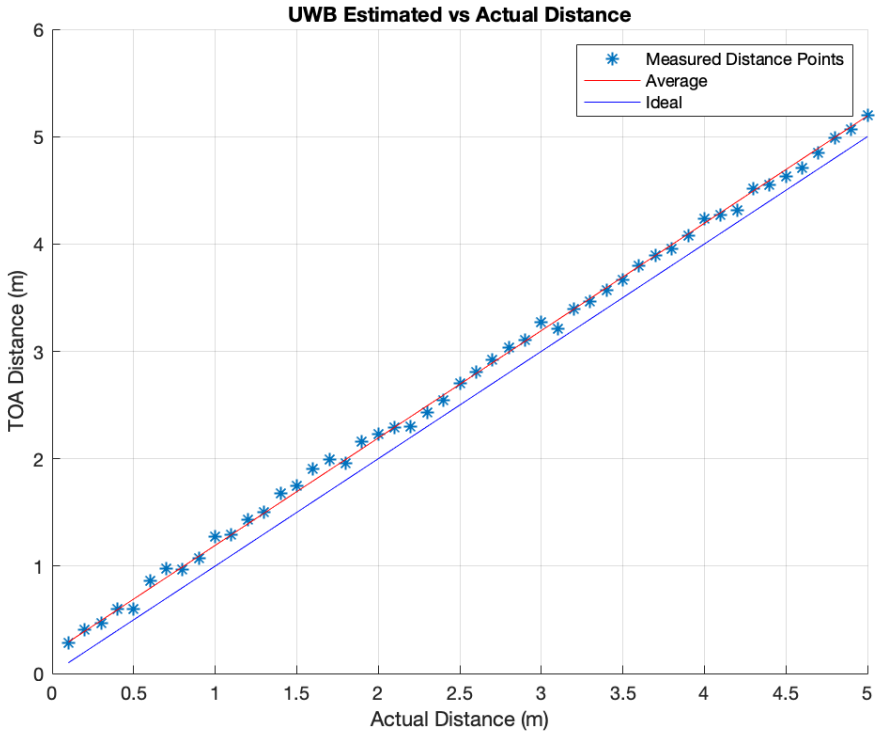

Figure 4.6: Distance derived from TOA of the first path versus the actual distance from the transmitter to the receiver when the datapoint was collected for UWB TOA ranging in LOS condition

The data points represent the distances that were both estimated and physically measured. The blue line represents the ideal case, in which the estimated distance would be exactly equal to the measured distance. The red line represents the average distance estimated at each increment and is parallel to the ideal as it should be.

The estimated distances are not exactly equal to the measured distances, but they are close. This suggests that distance estimations made using UWB are fairly accurate, though not perfect. It should also be noted that the data points do not form a perfectly straight line, and these fluctuations along the line can be attributed to the unsteadiness in path loss of the signal. The fact that the points are about equally spaced both above and below the red line indicated that their error likely follows a Gaussian distribution. Because the points are above the blue line, the distribution of errors is likely positively skewed to the left – which means that the distance estimation is very often greater than the actual measured distance. We believe this trend is due to our particular methodology and the physical properties of the test room environment.

The distance estimation error was then graphed and quantified, similar to the data collected during the BLE LOS methodology (Figure 4.7).

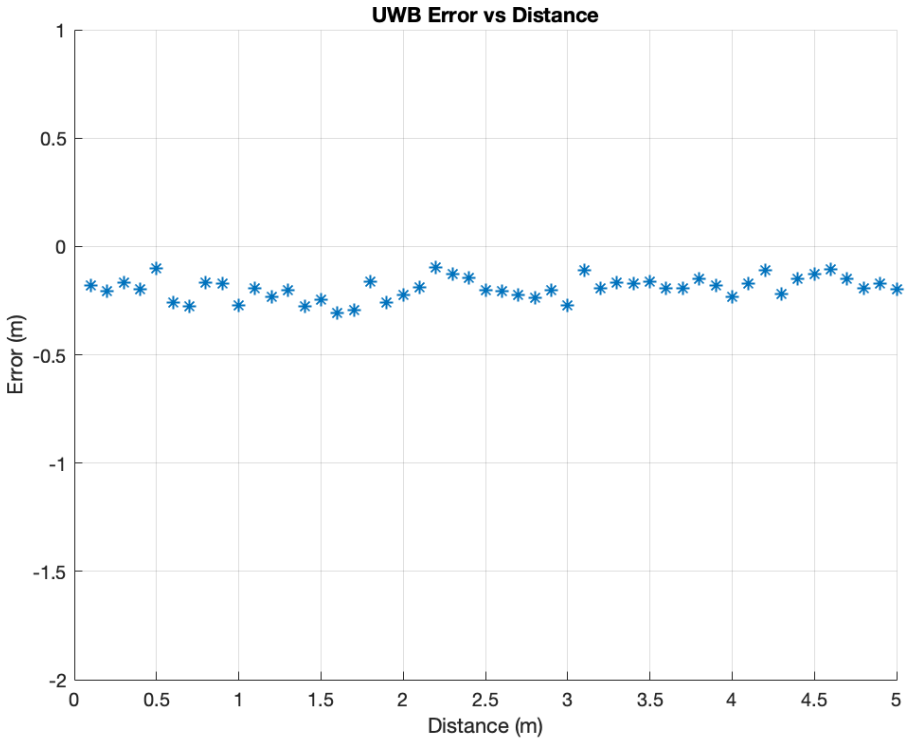

Figure 4.7: Distance errors versus the actual distance from the transmitter to the receiver when the datapoint was collected for UWB TOA ranging in LOS condition

Unlike the BLE Error versus Distance graph which showed a steady increase in error over distance, the data collected during the UWB LOS methodology shows an error that remains relatively constant as distance increases. This suggests that the error in UWB distance estimations is not related to distance, and that distance estimations made using UWB are more accurate than those made using BLE.

It should also be noted that the errors associated with these data points are much smaller than those which were observed in the BLE graphs. This supports the idea that UWB distance estimations are more accurate than those made using BLE.

A histogram of the data collected was created to analyze the effects of noise which are accounted for in Eq. 2.8 through the random variable η (Figure 4.8). Previous research makes the claim that η is random following a Gaussian distribution (Pahlavan, 2013).

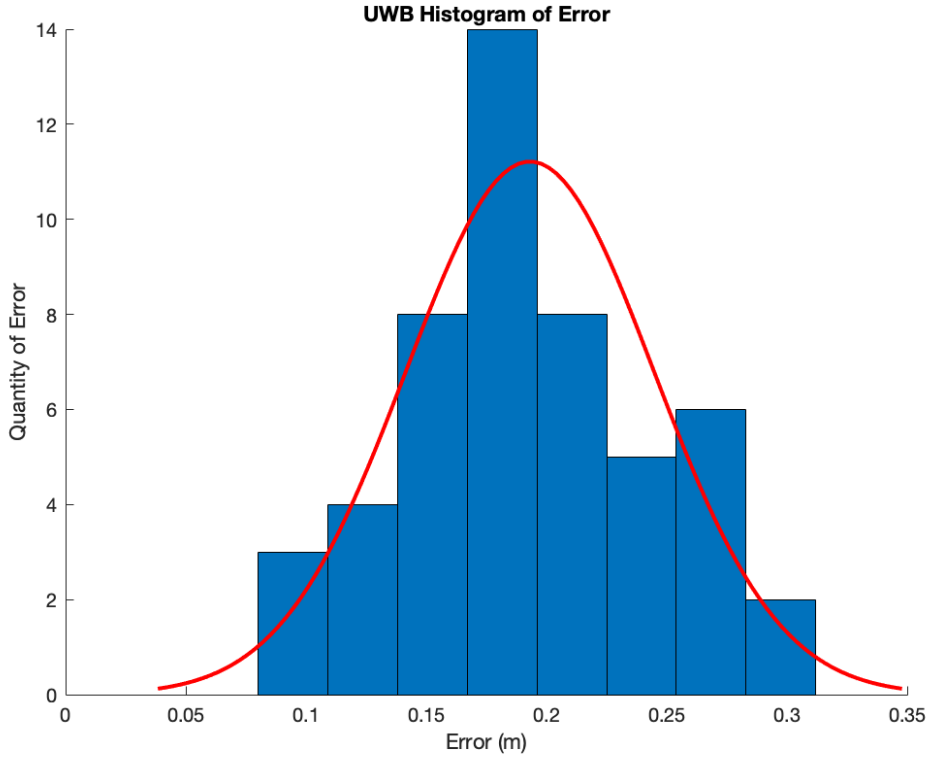

Figure 4.8: Histogram displaying the distance error versus the quantity of error for UWB TOA ranging in LOS condition

The data fits the Gaussian, or Normal, distribution, which can be seen by the curve drawn across the histogram. While the quantity of errors is not exactly symmetrical, the data is still a relatively good fit to the normal distribution, proving that the errors are randomly distributed following a Gaussian distribution.

Recall from Eq. 2.14, that the CRLB (CRLB) for UWB distance estimations can be calculated by using our data and associated methodology parameters. Equation 2.14 is used where the CRLB is represented by σ_d, c is the speed of light, SNR is the signal-to-noise ratio, and f_0 is the frequency at which the signal is pulsed.

In our case of CRLB measurement, we assume that measurement time is the same as symbol function where W x T_M = 1. Then, the standard deviation of ranging error can be calculated as:

$$\sigma_r \geq \frac{3 \times 10^8}{2\Pi\sqrt{2 \times 3.46 * 10^{-4} \times \left((6 \times 10^9)^2 + \frac{(5 \times 10^9)^2}{12}\right)}} \approx 0.33m$$

The CRLB of our UWB distance estimations is to be approximately 33cm. This means that in the *best* case, with minimum noise, our distance estimation may not be perfectly accurate, but UWB beacons are capable of estimating distances within about 33 centimeters.

We also calculated the variance of our distance estimations using the standard statistical equation for variance, the variance of our data set was found to be $\sigma = 0.413$m. It should be noted that the variance of the OLOS trials is greater than that of the LOS trials. This can be attributed to the greater error that is realized while our body obstructs the signal. While similar to the CRLB realized, spread of error found by using our data is much larger. This larger value is likely more accurate, because some estimations were made when calculating our CRLB, such as $W * T_M = 1$.

The CRLB can then be used to compare the two technologies, where the CRLB of distance estimations made with TOA is much less than those made with RSS, and TOA estimation error is independent of distance. This means that distance estimations made using UWB will be more accurate than those made using BLE.

4.2 OLOS Ranging Results

In this subsection, we display the results for both BLE and UWB ranging in OLOS condition. For the BLE results, we have graphs depicting RSS versus distance, graphs displaying actual distance versus measured distance, and graphs showing the ranging error versus distance specifically in OLOS condition. For the UWB results, we have graphs displaying the direct path's pathloss versus the distance derived from TOA, actual distance versus distance derived from TOA, distance error versus actual distance, as well as histograms to help visualize the quantity and distribution of the distance error. Overall, we can see that in OLOS condition the inaccuracy inherent in BLE ranging are further amplified by the effect of the blocking body. BLE ranging results in OLOS condition are rarely if ever reflective of the actual distance. On the other hand, while it is clear that UWB ranging results are also affected by the OLOS condition as well we can still get consistent accurate results with UWB ranging.

4.2.1 BLE Ranging in OLOS

The data collected during our BLE OLOS ranging study in LOS has been summarized in a scatter plot below (Figure 4.9). Each received signal is represented by a dot on the graph that describes its magnitude in dB and its measured distance from the transmitting antenna. A line-of-best-fit has been included to illustrate the trend in signal strength as a result of increasing distance. Refer to Appendix B for the full collection of data for the BLE OLOS trial.

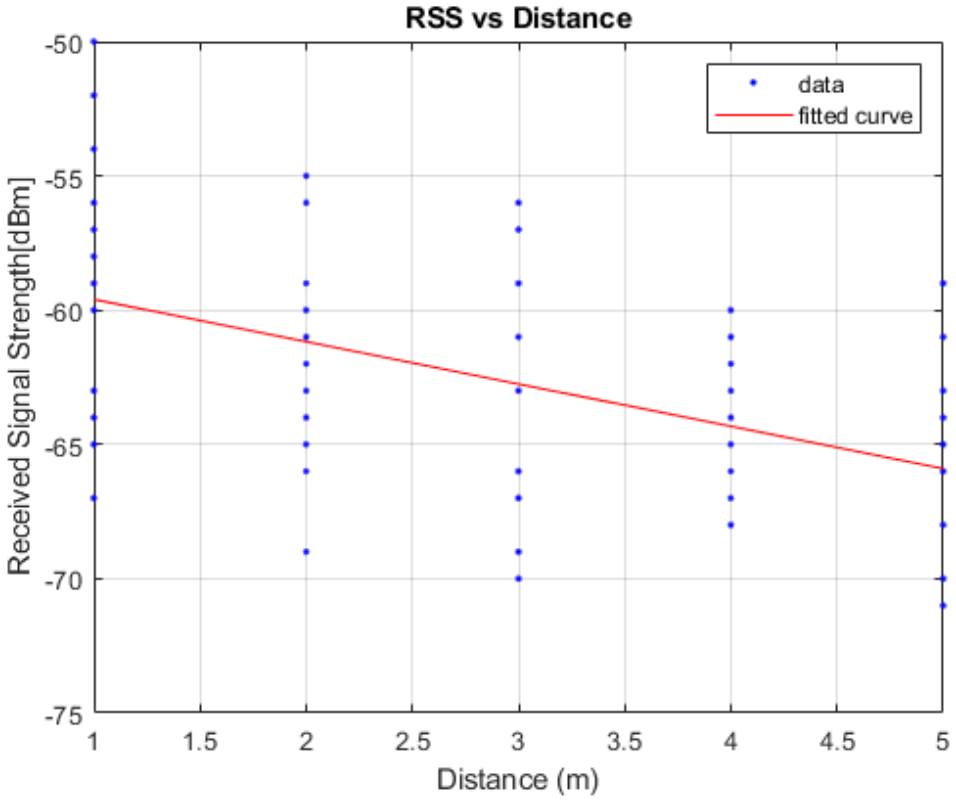

Figure 4.9: RSS versus distance in OLOS condition and the best fit line for path-loss modeling for BLE ranging

The trend line suggests that RSS and distance still share an inverse relationship in OLOS conditions, and that RSS decreases as distance increases.

With this in mind, Eq. 2.3 can be used to estimate the exact distance between the receiving and transmitting BLE antennas. To better understand these estimations, the error of all measurements taken at each distance was determined and summarized in the graph below (Figure 4.10).

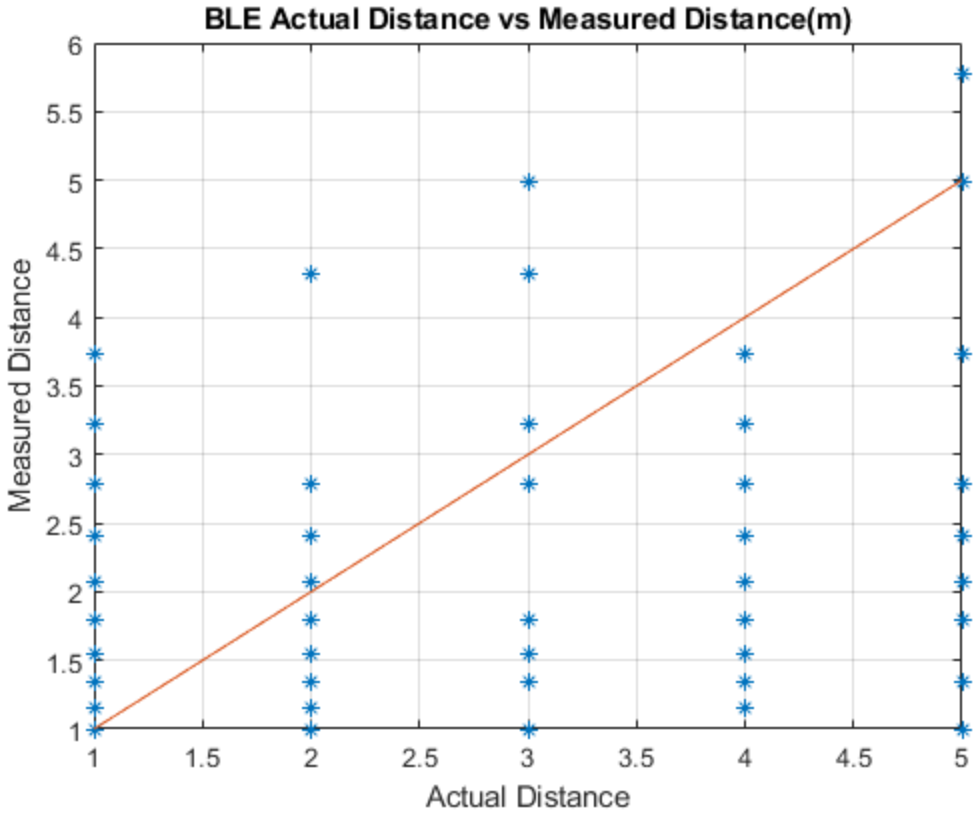

Figure 4.10: Actual distance versus measured distance in OLOS condition for BLE RSS ranging with the line representing the ideal distance measurement

Observing the data as represented above, a slight trend exists that supports that the error associated with distance estimations is directly related to the physical distance between the receiving and transmitting antennas. However, this trend is much weaker than previously seen in the LOS conditions. Under OLOS conditions, distance estimation error was *much* greater. The spread of data points at each distance increment indicates the accuracy of the distance estimations. As the spread of the data points (the range of distances) increases, the accuracy of the measurement decreases. It should be noticed that the data points are spread farthest apart at the longest distance. This change in spread, along with the depicted trend line supports the idea that as distance increases, the spread – and therefore, accuracy of distance estimations, decreases. However, in this particular case of OLOS conditions, the spread is generally high at every distance increment, suggesting that the RSS-based distance estimations will not be very accurate.

As discussed in Chapter 2.4.2, this change in error and accuracy can be fully quantified by using CRLB theory. In this context, the average error at each distance was considered, and the standard deviations of those errors were used to depict the CRLB (Figure 4.11).

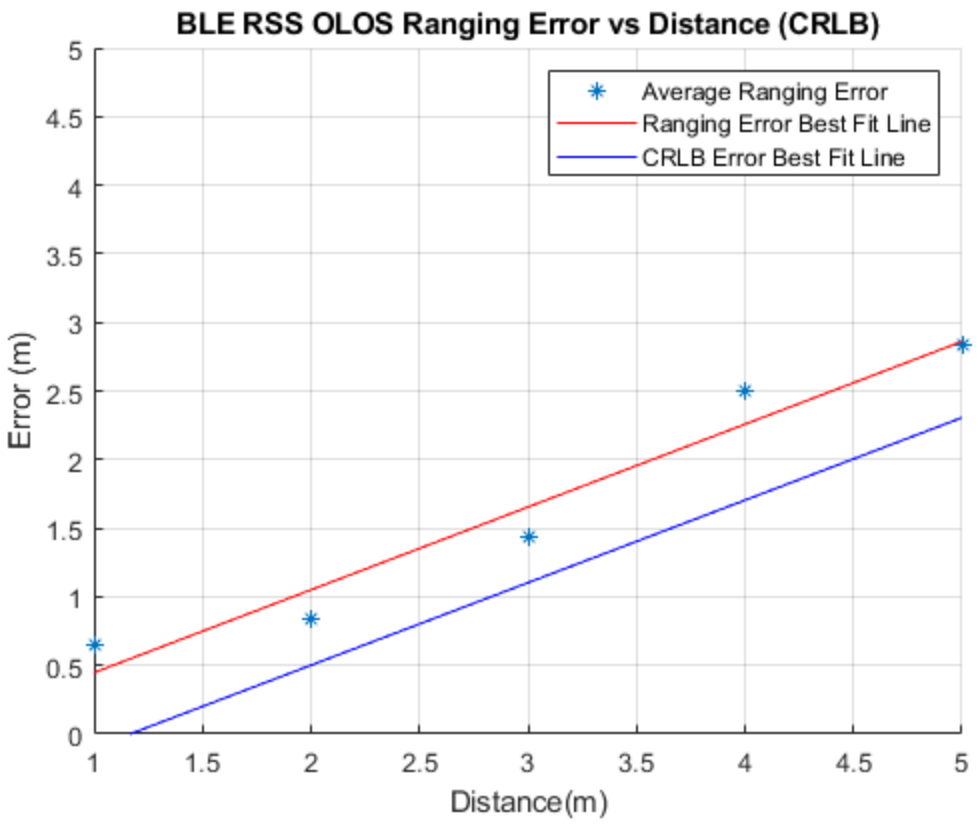

Figure 4.11: Ranging error versus distance in OLOS condition for BLE Ranging with the asterisks representing the average ranging error at a given distance while the two lines are the empirical and theoretical CRLB best fit curve respectively

The data points depict the standard deviation of the distance estimations made at each location. The red line shows the general trend of those standard deviations, and its positive slope suggests that the standard deviation of error increases as distance between the transmitting and receiving antennas increases.

Using MATLAB and Eq. 2.3, the CRLB was calculated using this data and is depicted by the blue line on the graph. The CRLB considers the best-case scenario, where shadow fading effects are minimized. The standard deviation of error, which maps accuracy with the consideration of shadow fading, represents the accuracy bound we should really expect.

In this case, the CRLB is dependent on the distance, which can be assumed because it changes as distance changes. At the closest distance of 1m, the CRLB was calculated to be about 0.1002m, and at the farthest distance, the CRLB was found to be 2.506m. This means that the *best* performance we can expect from our BLE distance estimation methodology can only be correct within 0.1002m of the actual measured distance when the transmitting and receiving antennas are 1m apart. Likewise, the *best* performance we can expect when the transmitting and receiving antennas are 5m apart can only be correct within 2.506m of the actual measured distance. It should be noted that these values are higher than those of the BLE data collection in LOS conditions. This makes sense because the presence of our bodies directly contributes to the effects of shadow fading.

The OLOS BLE methodology explains that both the accuracy of distance estimations in an enclosed meeting room environment are dependent on the ranging distance between the transmitting and receiving antennas. It also suggests that BLE measurements are more accurate under LOS conditions, as opposed to OLOS conditions.

4.2.2 UWB Ranging in OLOS

Apart from measuring LOS for TOA of UWB, we also measured how the signal would be affected in OLOS conditions. The first-path path loss of the waveforms collected during this procedure were considered and, the Eq. 2.8 was used to produce a graph which depicts TOA first-path path loss versus distance (Figure 4.12).

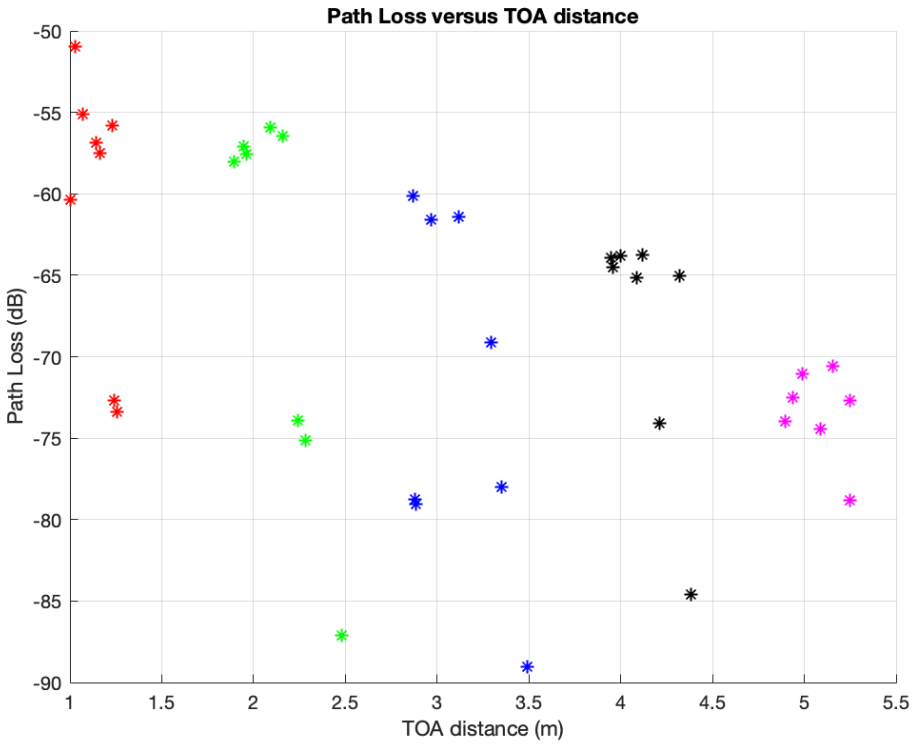

Figure 4.12: Path loss of the direct path versus distance derived from TOA of the direct path for UWB TOA ranging in OLOS condition with 8 measurement taken every meter, each Measurement taken with the blocking subject in a different orientation

Recall from Eq. 2.2 that the relationship between TOA and UWB distance estimations can be described by $d = \tau \times c$. The TOA data points gathered from the waveforms are representative of τ. By simply multiplying each point by the speed of light, c, we can depict the relationship between estimated distance and TOA path loss.

The various colors on the graph represent the data points collected at each of the five distance increments (1m, 2m, 3m, 4m, and 5m). A general trend can be identified where many of the data points at

a certain distance increment appear clustered, and a couple outlying points appear with much higher path loss. The largest cluster of points represents the data collected during our 360° spin, where our bodies did not block the LOS between the transmitting and receiving antennas. The outlying points that experience greater path loss are representative of the few data points which were collected while our bodies obstructed the LOS.

Our data suggests that a relationship between TOA and Signal Strength in which they are proportional. The trend in which the points gradually slope downward illustrates that the magnitude of path loss increases as the distance between the transmitting and receiving antennas increases. This is supported by Eq. 2.8, which describes the theoretical relationship between observed power at the transmitting antenna, O(t), and the TOA, τ.

After verifying our data, we assessed its accuracy for distance estimating. We created a graph which depicts the estimated distance using TOA, versus the actual measured distance. Ideally, this curve should be represented as a straight line with a slope of 1, which suggests that the distance estimated by TOA is always equal to the actual measured distance (Figure 4.13).

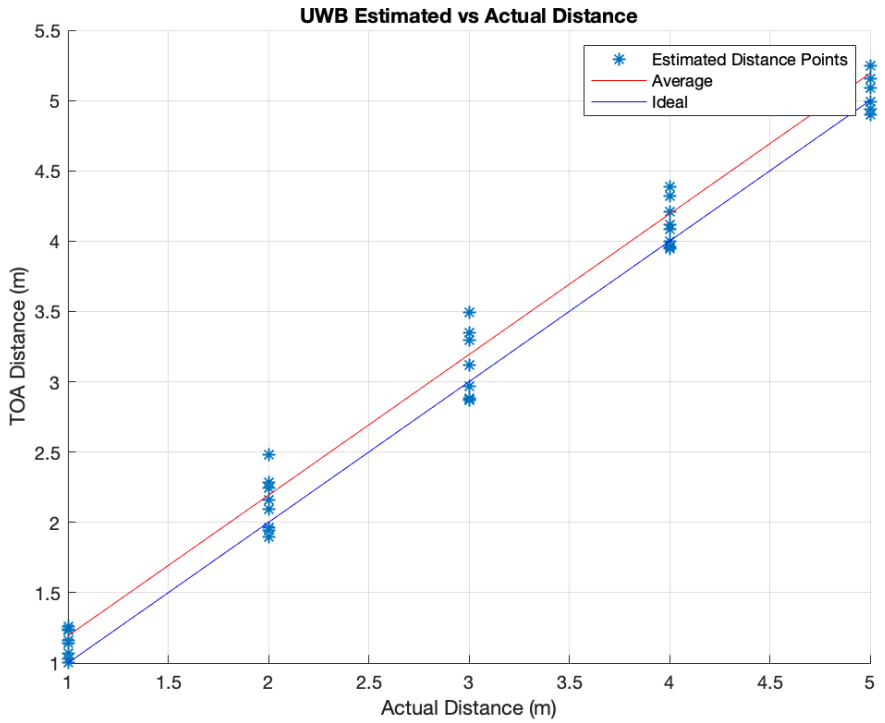

Figure 4.13: Distance derived from TOA of the first path versus the actual distance from the transmitter to the receiver when the datapoint was collected for UWB TOA ranging in OLOS condition

The data points represent the distances that were both estimated and physically measured. The blue line represents the ideal case, in which the estimated distance would be exactly equal to the measured distance. The red line represents the average distance estimated at each increment and is parallel to the ideal as it should be.

The estimated distances are not exactly equal to the measured distances, but they are close. This suggests that distance estimations made using UWB are fairly accurate, though not perfect. It should also be noted that the data points do not form a perfectly straight line, and these fluctuations along the line can be attributed to the unsteadiness in path loss of the signal. The fact that the points are about equally spaced both above and below the red line indicated that their error likely follows a Gaussian distribution. Because the points are above the blue line, the distribution of errors is likely positively skewed to the left – which means that the distance estimation is very often greater than the actual measured distance. We believe this trend is due to our particular methodology and the physical properties of the test room environment.

The distance estimation error was then graphed and quantified, similar to the data collected during the BLE LOS methodology (Figure 4.14).

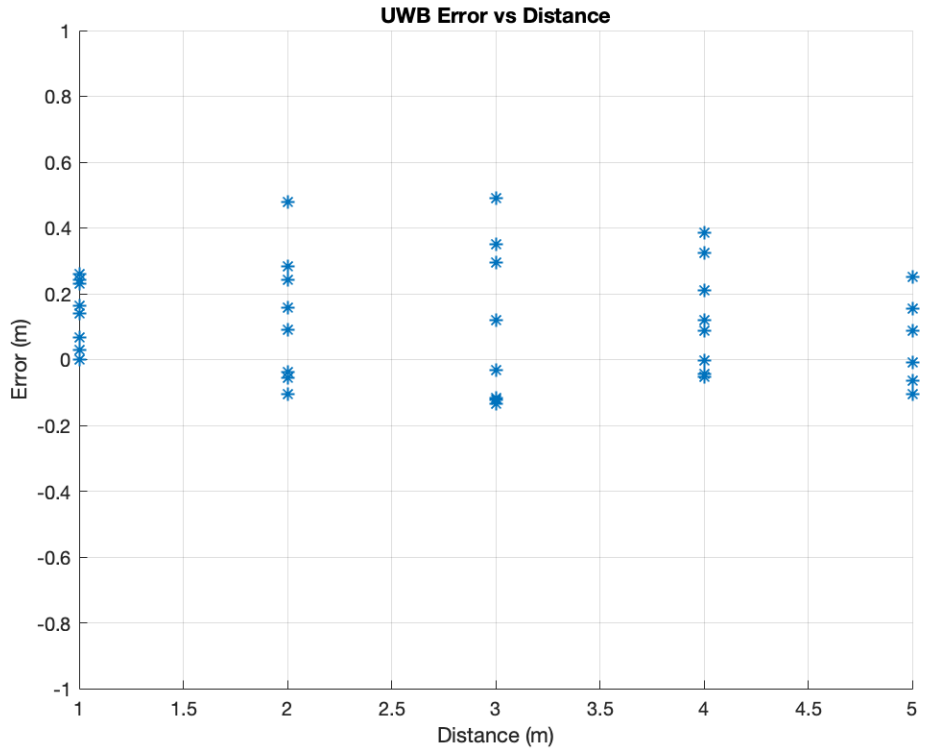

Figure 4.14: Distance errors versus actual distance from the transmitter to the receiver when the data point was collected for UWB TOA ranging in OLOS condition

Unlike the BLE Error versus Distance graph which showed a steady increase in error over distance, the data collected during the UWB LOS methodology shows an error that remains relatively constant as distance increases. This suggests that the error in UWB distance estimations is not related to distance, and that distance estimations made using UWB are more accurate than those made using BLE, even when the LOS is obstructed.

It should also be noted that the errors associated with these data points are much smaller than those which were observed in the BLE – OLOS graphs. This supports the idea that UWB distance estimations made in OLOS conditions are more accurate than those made using BLE in those same conditions.

A histogram of the data collected was created to analyze the effects of white noise which are accounted for in Eq. 2.8 through the random variable η (Figure 4.15). Previous research makes the claim that η is random following a Gaussian distribution (Pahlavan 2013).

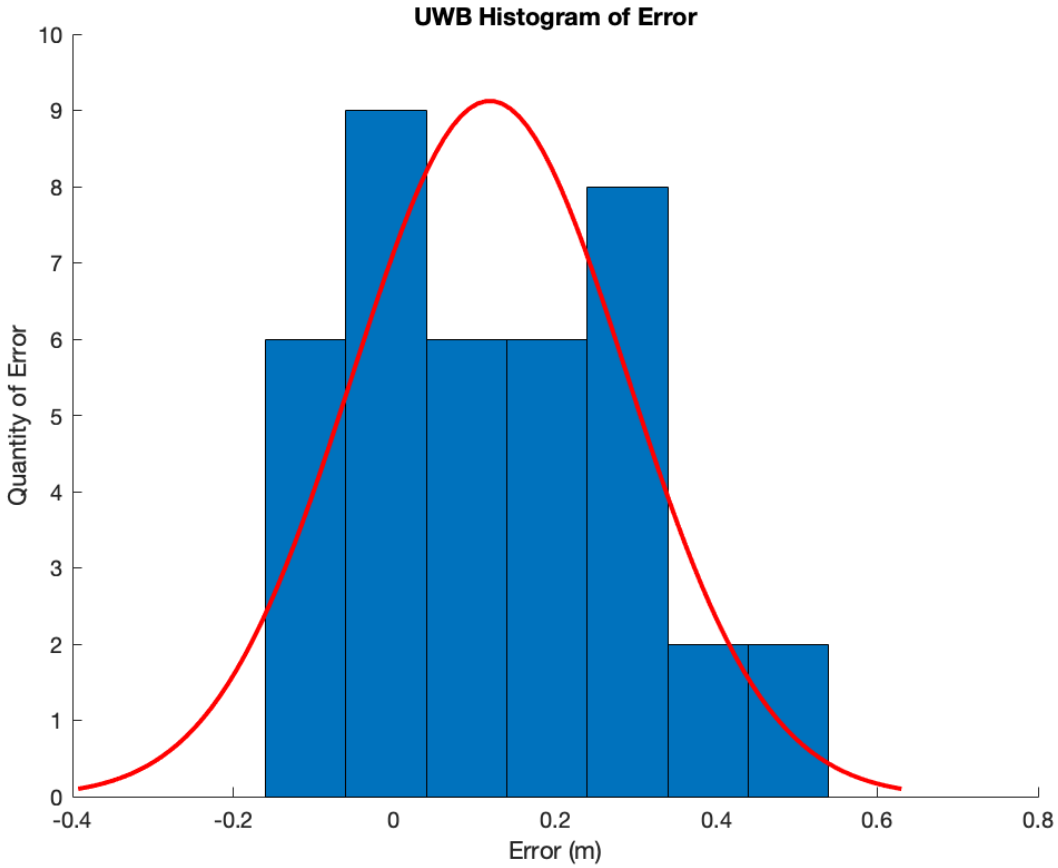

Figure 4.15: Histogram displaying the distance error versus the quantity of error for UWB TOA ranging in OLOS condition

The data fits the Gaussian, or Normal, distribution, which can be seen by the curve drawn across the histogram. While the quantity of errors is not exactly symmetrical, the data is still a relatively good fit to the normal distribution, proving that the errors are randomly distributed following a Gaussian distribution.

Recall from Eq. 2.14, that the CRLB (CRLB) for UWB distance estimations can be calculated the same way it was during the LOS trials, and the CRLB remains approximately 33cm. This means that in the *best* case, with minimum noise, our distance estimation may not be perfectly accurate, but UWB beacons are capable of estimating distances within about 33 centimeters.

$$\sigma_r \geq \frac{3 \times 10^8}{2\Pi\sqrt{2\times3.46*10^{-4}\times\left((6\times10^9)^2+\frac{(5\times10^9)^2}{12}\right)}} \approx 0.33m$$

We also calculated the variance of our OLOS distance estimations using the standard statistical equation for variance, the variance of our data set was found to be $\sigma = 0.467$m. While similar to the CRLB realized, spread of error found by using our data is much larger. This larger value is likely more accurate, because some estimations were made when calculating our CRLB, such as $W * T_M = 1$.

The CRLB can then be used to compare the two technologies, where the CRLB of distance estimations in OLOS conditions made with TOA is much less than those made with RSS, and TOA OLOS estimation error is independent of distance. This means that distance estimations made using UWB will be more accurate than those made using BLE, even under OLOS conditions.

Figure 20 shows the CRLB of the UWB shadowing and the graph line shows an almost straight line hanging around 0.2m. Histogram of error is shown in Figure 21 below.

By comparing this result with the CRLB of BLE, we can conclude that UWB is much more accurate. With a *minimum* variance of about 0.5m, the accuracy of BLE technology pales in comparison to UWB which shows a *maximum* variance of 39.9mm. The difference is statistically significant at a value of 0.46m. Because the minimum variance of our BLE estimations is still larger than the maximum of our UWB measurements, we can conclude that distance estimations made using UWB are more accurate than those made using BLE. This also suggests that UWB positioning should produce results that are more accurate than BLE positioning because they will be based on more accurate distance estimations.

4.3 Positioning Results

In this section, we use the ranging errors in OLOS and LOS condition for UWB and BLE to derive the positioning error in a 5.7 x 5.7 m room with 5 total access points, 1 in the middle of the room and the other 4 on each of the wall's middle point. The positioning errors are displayed through heat maps of the error contour as well as the CDF of error in OLOS and LOS for both UWB and BLE. Overall, for both the BLE and UWB positioning, the positioning error are reflective of the ranging error. Furthermore, we can see that the ranging error also generally agrees with results from previous studies. Aside from that, comparing our theoretical results and empirical results also show that reality is often disappointing.

4.3.1 BLE LOS versus OLOS

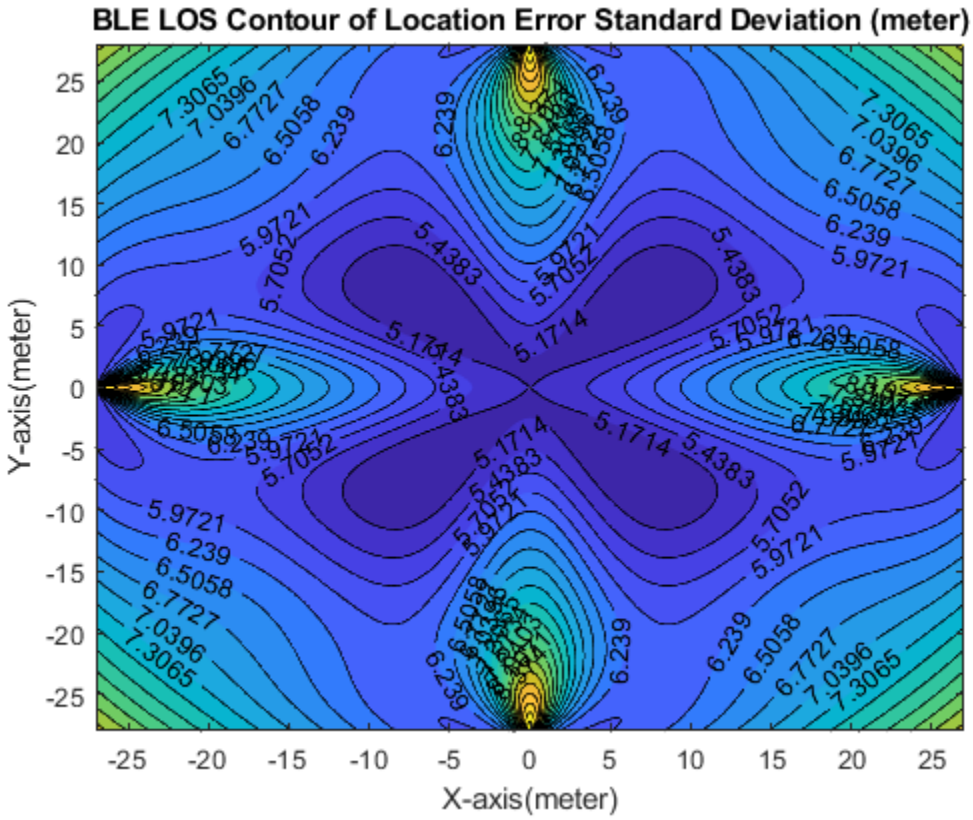

Figure 4.16: BLE LOS contour of location error heat map in cm for a 5.7 x 5.7 m room with access points in the middle of the room and the middle of each wall

The figure shown above display the contour of BLE-RSS based indoor localization errors in an approximately 5.7 x 5.7 m room. The alpha value (α), or the distance power gradient of the path-loss model that we come up with earlier is $\alpha = 2.211$ while the standard deviation of shadow fading (σ) that we got from our calculation and measurement is $\sigma = 2.5525$ dB. In this specific scenario, we assumed that 5 access points was used, with 4 in the middle of each of the room's walls and one in the center of the room. Overall, we realized that our results generally agree with results from earlier studies (Pahlavan, 2013) in that the variance of position error is higher along the sidelines of the area of concerned, particularly the middle section of the walls as well as in the corners of the room while the variance of position error is lower in near the center area of the room. From this graph, we can see that generally, the positioning error is close to the ranging error that we mentioned above. Furthermore, it can also be observed that the ranging error as well as the distance from the access point directly affects the positioning error.

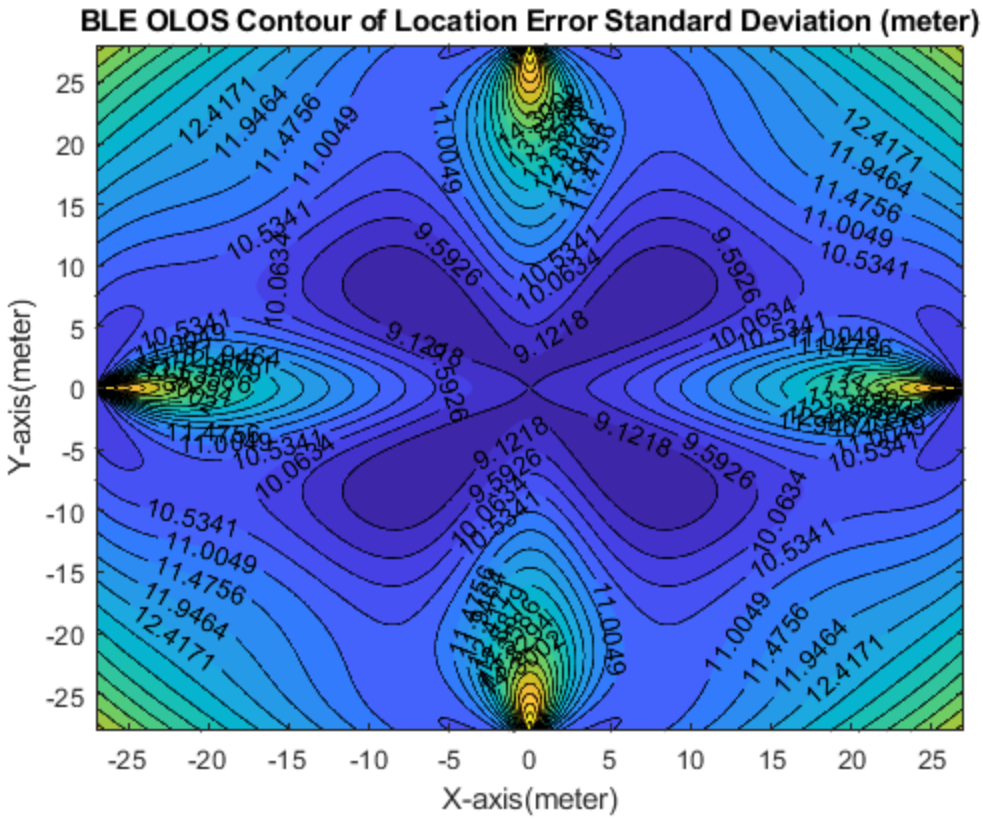

Figure 4.17: BLE OLOS contour of location error heat map in cm for a 5.7 x 5.7 m room with access points in the middle of the room and the middle of each wall

The figure shown above display the contour of BLE-RSS based indoor localization errors in an approximately 5.7 x 5.7 m room. The alpha value (α), or the distance power gradient of the path-loss model that we come up with earlier is $\alpha = 2.211$ while the standard deviation of shadow fading (σ) that we got from our calculation and measurement is $\sigma = 4.5094$ dB. In this specific scenario, we assumed that 5 access points was used, with 4 in the middle of each of the room's walls and one in the center of the room. Overall, we realized that our results generally agree with results from earlier studies (Pahlavan, 2013) in that the variance of position error is higher along the sidelines of the area of concerned, particularly the middle section of the walls as well as in the corners of the room while the variance of position error is lower in near the center area of the room. From this graph, we can see that generally, the positioning error is close to the ranging error that we mentioned above. Furthermore, it can also be observed that the ranging error as well as the distance from the access point directly affects the positioning error.

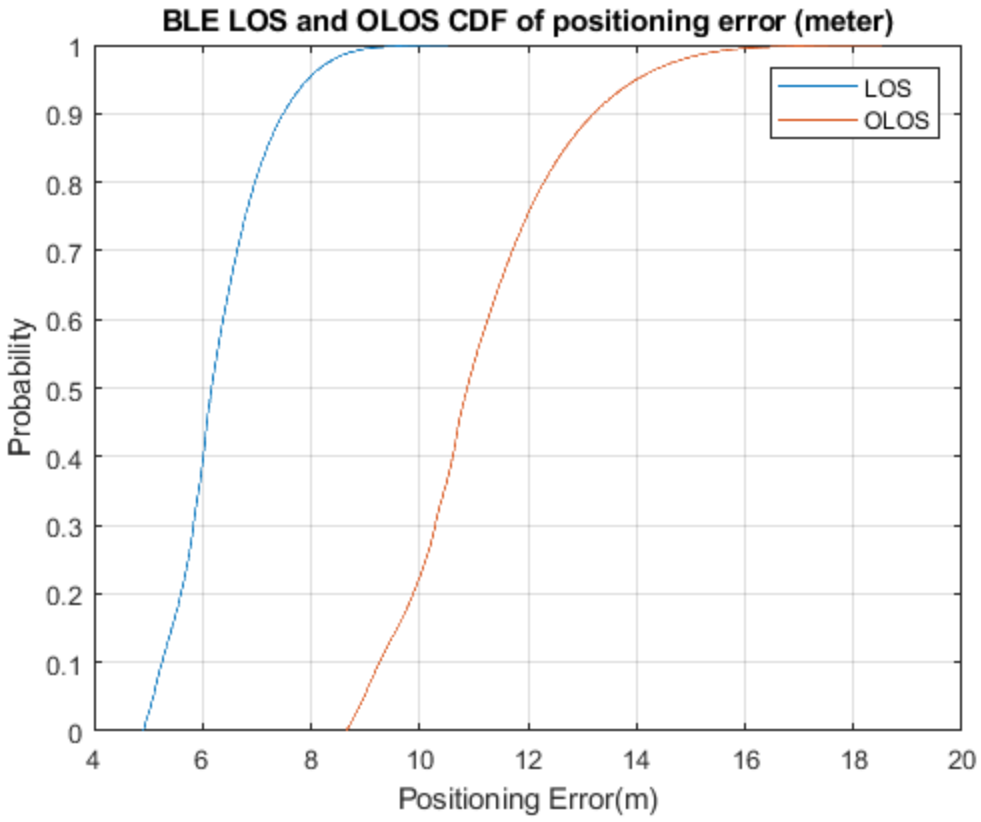

Figure 4.18: Comparison of BLE LOS and OLOS CDF of positioning error in a 5.7 x 5.7 m room with access points in the middle of room and the middle of each wall

From the graph above, we can clearly see that the positioning error for both LOS and OLOS scenario are generally close to our ranging error. With the maximum positioning error for LOS is around 8 while that for OLS is around 16. Thus, we can see that the positioning error for OLOS scenario is significantly higher than that for LOS scenario, which also generally agrees with our ranging results for OLOS and LOS respectively. Another noteworthy fact is that the positing error for BLE-RSS systems are quite high (usually approximately 15 – 20% the dimension of the room) and thus it would be very difficult for a BLE-RSS to accurately locate the position of a receiver.

4.3.2 UWB LOS versus OLOS

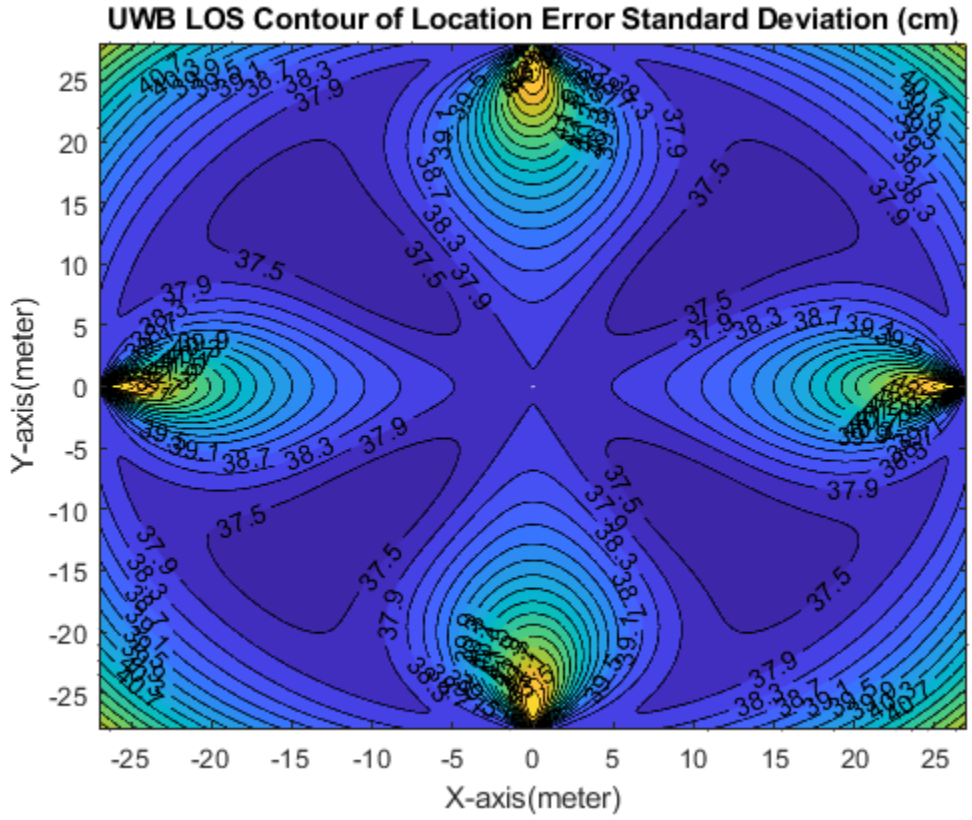

Figure 4.19: UWB LOS contour of location error heat map in cm for a 5.7 x 5.7 m room with access points in the middle of room and the middle of each wall

The figure shown above display the contour of UWB-TOA based indoor localization errors in an approximately 5.7 x 5.7 m room. The ranging error is determined to be about 0.413 m or 41.3 cm, while the standard deviation of measurement time that we got from our calculation and measurement is determined to be about 1.1 ns. In this specific scenario, we assumed that 5 access points was used, with 4 in the middle of each of the room's walls and one in the center of the room. Overall, we realized that the variance of position error is higher along the sidelines of the area of concerned, particularly the middle section of the walls as well as in the corners of the room. Also, the variance of position error is lower in near the center area of the room and it is especially low in the four diagonals of the room. From this graph, we can see that generally, the positioning error is close to the ranging error that we mentioned above. Furthermore, it can also be observed that the ranging error as well as the distance from the access point directly affects the positioning error much like in the case of the BLE-RSS based results.

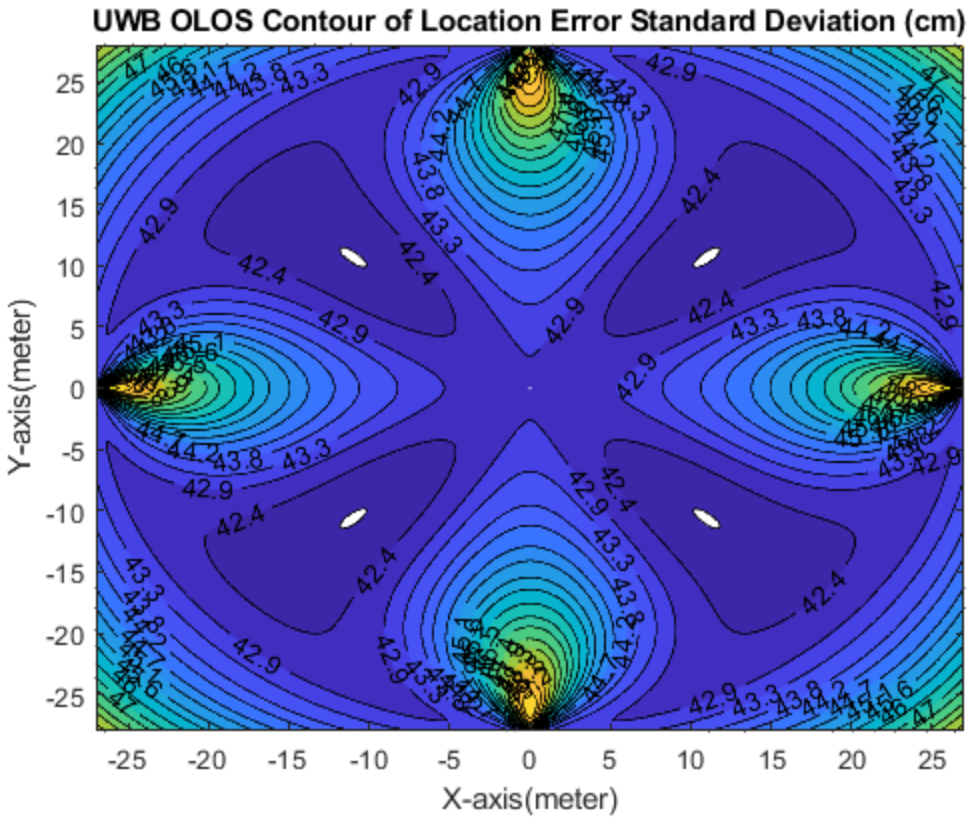

Figure 4.20: UWB OLOS contour of location error heat map in cm for a 5.7 x 5.7 m room with access points in the middle of room and the middle of each wall

The figure shown above display the contour of UWB-TOA based indoor localization errors in an approximately 5.7 x 5.7 m room. The ranging error for OLOS, which we get from our measurements, is about 46.7 cm, while the standard deviation of measurement time that we got from our calculation and measurement is determined to be about 1.23 ns. In this specific scenario, we assumed that 5 access points was used, with 4 in the middle of each of the room's walls and one in the center of the room. Overall, we realized that the variance of position error is higher along the sidelines of the area of concerned, particularly the middle section of the walls as well as in the corners of the room. Also, the variance of position error is lower in near the center area of the room and it is especially low in the four diagonals of the room. From this graph, we can see that generally, the positioning error is close to the ranging error that we mentioned above. Furthermore, it can also be observed that the ranging error as well as the distance from the access point directly affects the positioning error much like in the case of the BLE-RSS based results.

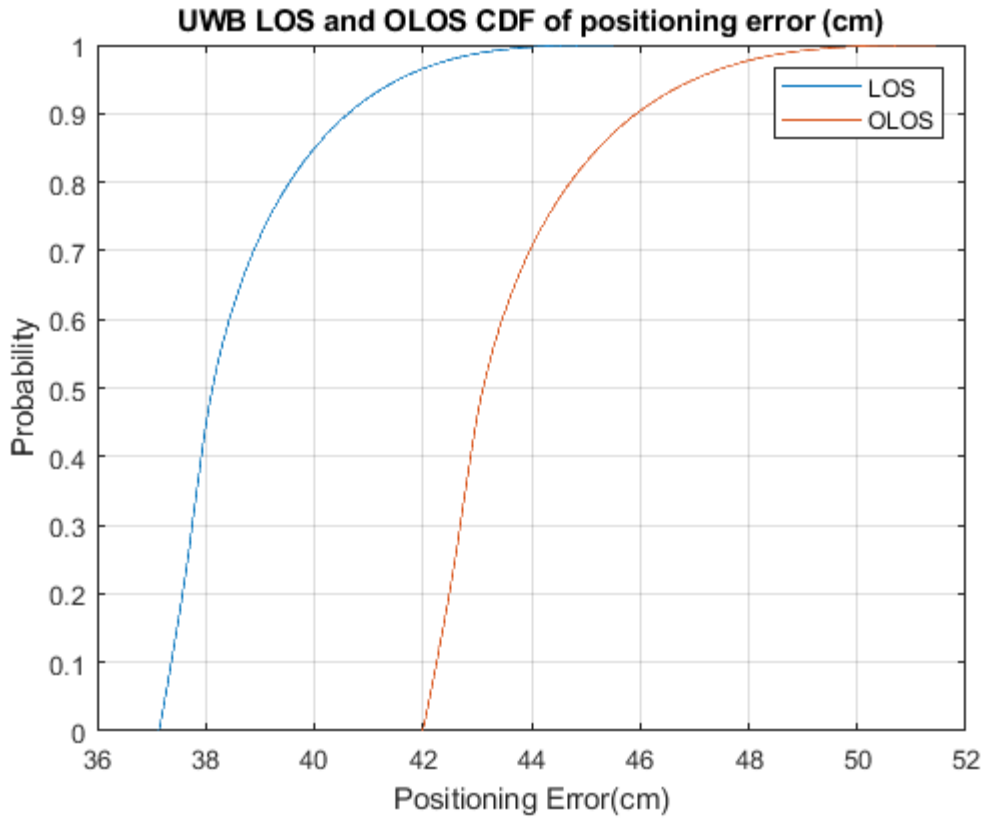

Figure 4.21: Comparison of UWB LOS and OLOS CDF of positioning error in a 5.7 x 5.7 m room with access points in the middle of room and the middle of each wall

From the graph above, we can clearly see that the positioning error for both LOS and OLOS scenario are generally close to our ranging error. With the maximum positioning error for LOS is around 41.3 cm while that for OLOS is around 46.7 cm. Thus, we can see that the positioning error for OLOS scenario is significantly higher than that for LOS scenario, which also generally agrees with our ranging results for OLOS and LOS respectively. Furthermore, the fact the positioning error for UWB-TOA systems are measured in cm while that of BLE-RSS systems are measured in m speak volumes about the discrepancies between the two types of system.

4.3.3 UWB CRLB versus Empirical

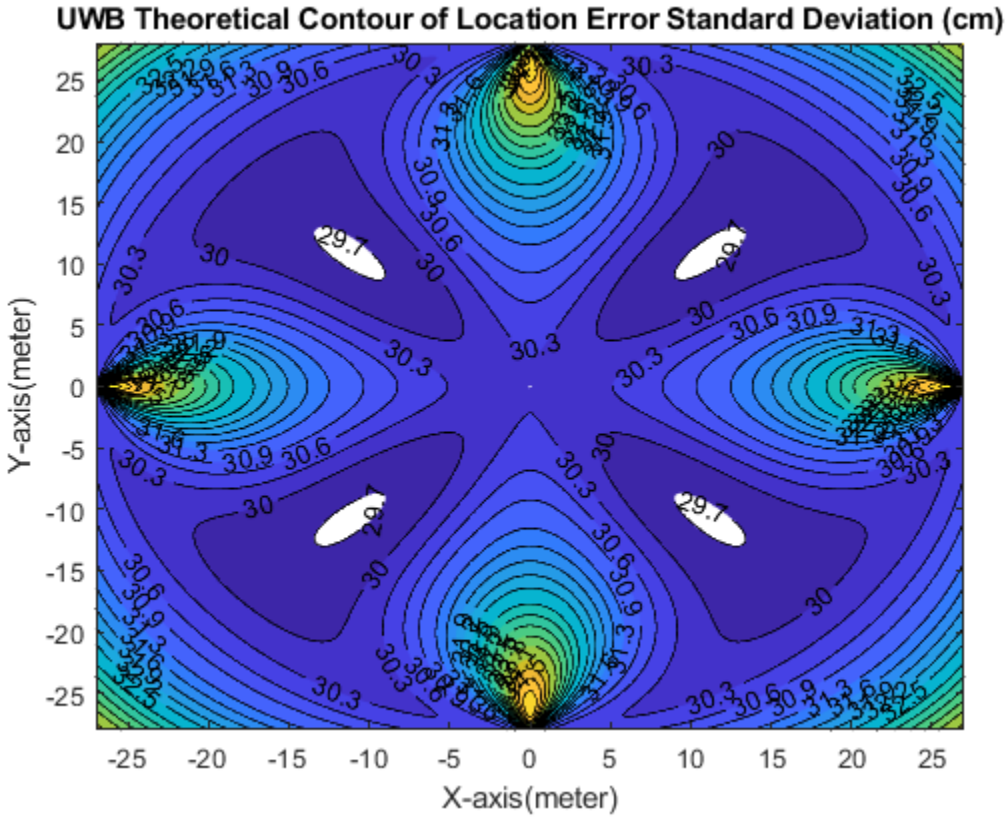

Figure 4.22: UWB theoretical CRLB contour of location error heat map in cm for a 5.7 x 5.7 m room with access points in the middle of room and the middle of each wall

The figure shown above display the contour of UWB-TOA based indoor localization errors in an approximately 5.7 x 5.7 m room. The ranging error (CRLB), shown in the calculations above, is determined to be about 33 cm, while the standard deviation of measurement time that we got from our calculation and measurement is determined to be about 1.1 ns. In this specific scenario, we assumed that 5 access points was used, with 4 in the middle of each of the room's walls and one in the center of the room. Overall, we realized that the variance of position error is higher along the sidelines of the area of concerned, particularly the middle section of the walls as well as in the corners of the room. Also, the variance of position error is lower in near the center area of the room and it is especially low in the four diagonals of the room. From this graph, we can see that generally, the positioning error is close to the ranging error that we mentioned above. Furthermore, it can also be observed that the ranging error as well as the distance from the access point directly affects the positioning error much like in the case of the BLE-RSS based results.

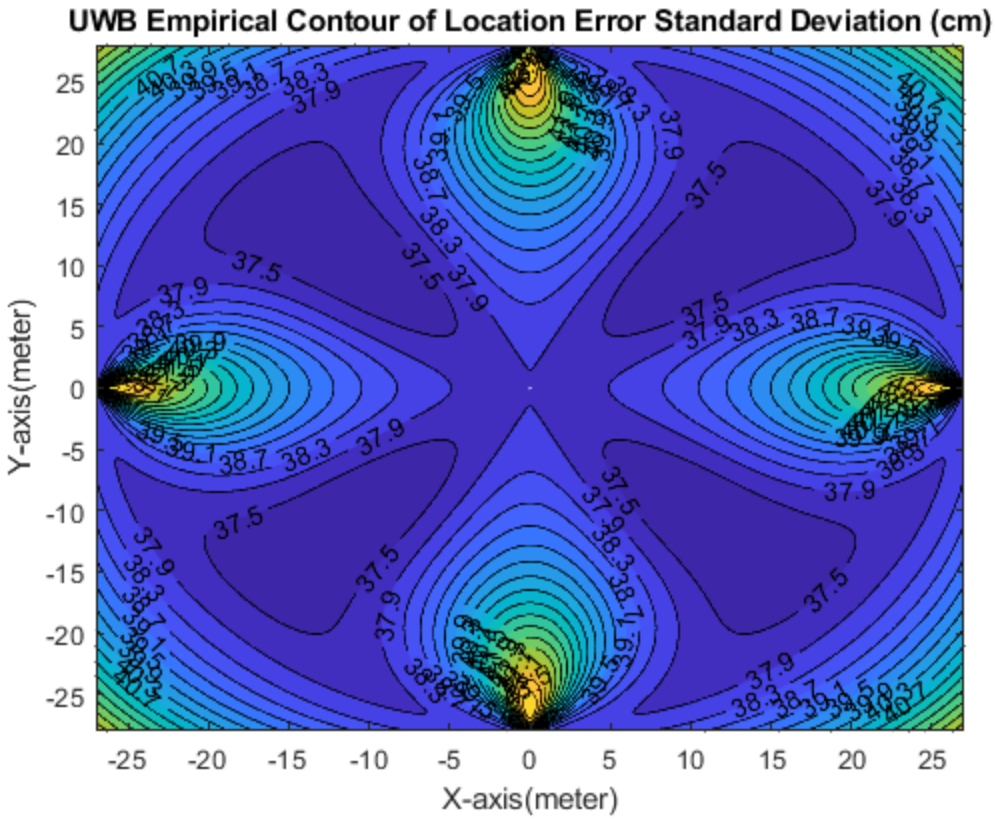

Figure 4.23: UWB empirical contour of location error heat map for a 5.7 x 5.7 m room with access point in the middle of the room and the middle of each wall

The figure shown above display the contour of UWB-TOA based indoor localization errors in an approximately 5.7 x 5.7 m room. The ranging error that we got from our measurements is determined to be about 41.3 cm, while the standard deviation of measurement time that we got from our calculation and measurement is determined to be about 1.1 ns. In this specific scenario, we assumed that 5 access points was used, with 4 in the middle of each of the room's walls and one in the center of the room. Overall, we realized that the variance of position error is higher along the sidelines of the area of concerned, particularly the middle section of the walls as well as in the corners of the room. Also, the variance of position error is lower in near the center area of the room and it is especially low in the four diagonals of the room. From this graph, we can see that generally, the positioning error is close to the ranging error that we mentioned above. Furthermore, it can also be observed that the ranging error as well as the distance from the access point directly affects the positioning error much like in the case of the BLE-RSS based results. It is worth noting that the empirical error is much higher than the predicted error. Since we used many assumptions when we calculated the CRLB, it is expected that the actual positioning error will me much larger. We can attribute the differences to a number of causes including imperfect measurement tools, inadequate shielding on the connectors of the VNA and low TX power.

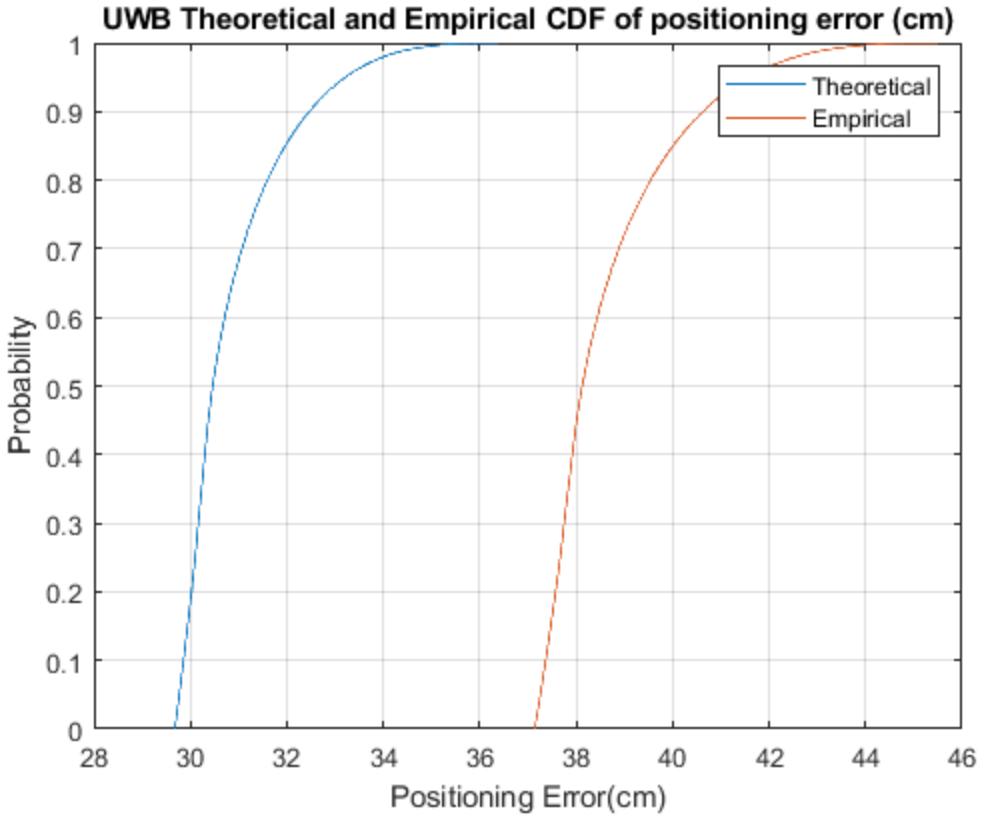

Figure 4.24: Comparison of UWB theoretical CRLB and empirical CDF of positioning error in a 5.7 x 5.7 m room with access points in the middle of room and the middle of each wall

From the graph above, we can clearly see that the positioning error for the empirical is much higher than our predicted value. The CRLB value which generally agrees with the ranging error, but we also expected that the empirical value will be much higher than the predicted CRLB value. The maximum error for the calculated CRLB is about 33 cm but that for the measured (empirical) value is about 41.3 cm. Another noteworthy fact is that the positing error for UWB-TOA systems are very low (usually only approximately 0.06 – 0.1% the dimension of the room) and thus it would offer much better accuracy than BLE-RSS systems. Even if the measured positioning error is more representative of UWB-TOA systems, the error is much lower than that of BLE-RSS systems. Furthermore, the fact the positioning error for UWB-TOA systems are measured in cm while that of BLE-RSS systems are measured in m speak volumes about the discrepancies between the two types of system.

5. Conclusions and Future Work

While the technology to navigate and localize in open, outdoor area has been established, there has been a need for indoor positioning and navigation technology. Indoor positioning serves a variety of purposes including businesses in warehouses, product location inside the stores, and in-home automation services. There is a lot of potential for such a technology, however it is very much in its infancy state with no set standards from manufacturers and regulators. Through this project, we explored the feasibility of the use of wireless beacons, particularly those equipped with BLE and UWB radios, for the use of indoor positioning.

Our primary goal was to compare BLE and UWB ranging accuracy to better understand their respective performance capabilities with respect to positioning. For both BLE and UWB, we focused on ranging in both LOS, where the room is empty, and OLOS, where furniture and other materials are present in the room. Based on our data analysis of these scenarios, we found that ranging for UWB provided more accurate distance estimations when compared to BLE in both LOS and OLOS cases. BLE distance estimations decrease in accuracy as distance between the transmitter and receiver increases. This is because the technology uses RSS-based ranging where the shadow facing component of the distance estimating algorithm is distance dependent. UWB, however, estimates distance using TOA, which is independent of the distance between the transmitter and receiver.

UWB and BLE are both viable localization options and should be considered for specific applications. Because of UWB's high accuracy, it is best suited for applications that require virtually exact location information such as VR gaming, or in military applications. BLE, however, is more user friendly since it has had the opportunity to mature in the market and is very well-suited for proximity-based applications like automated shopping or interactive museums.

While ranging alone cannot determine exact location, it lays the groundwork for the positioning algorithms need for localization. After completing our in-room ranging analysis, we suggest the results be used to further study the performance of BLE and UWB in actual positioning applications. Additional antennas and equipment can be purchased to map a room and relay coordinate location to the user using our research.

Appendix A: Complete Technical Specifications of Estimote® Location Beacons

TABLE A.1: COMPLETE TECHNICAL SPECIFICATIONS OF ESTIMOTE® LOCATION BEACONS

Identification (Hardware revision)	F3.3
MCU	Bluetooth® SoC ARM® Cortex®-M4 32-bit processor with FPU 64 MHz Core speed 512 kB Flash memory 64 kB RAM memory
Radio: 2.4 GHz transceiver	Bluetooth® 4.2 LE standard Range: up to 200 meters (650 feet) Output Power: -20 to +4 dBm in 4 dB steps, “Whisper mode” -40 dBm, "Long range mode" +10 dBm Sensitivity: -96 dBm Frequency range: 2400 MHz to 2483.5 MHz No. of channels: 40 Adjacent channel separation: 2 MHz Modulation: GFSK (FHSS) Antenna: PCB Meander, Monopole Antenna Gain: 0 dBi Over-the-air data rate: 1 Mbps (2 Mbps supported)
Sensors	Motion sensor (3-axis) Temperature sensor Ambient Light sensor Magnetometer (3-axis) Pressure sensor EEPROM Memory 1 Mb

	RTC clock
Additional features	GPIO NFC
Power Supply	4 x CR2477 – 3.0V lithium primary cell battery (replaceable) High efficient Step-Down DC-DC converter
Environmental Specification	Operating Temperature: 0°C to 60°C (32°F to 140°F) Storage Temperature (recommended): 15°C to 30°C (59°F to 86°F) Relative Humidity (operating): 20% to 80% relative humidity Relative Humidity (storage): 10% to 90% relative humidity, non-condensing Splash-proof
Materials	non-flammable enclosure: silicone adhesive layer: double-sided adhesive tape
Size and Weight	Length: 62.7 mm (2.47 inches) Width: 41.2 mm (1.62 inches) Height: 23.6 mm (0.93 inches) Weight: 67g (2.36 ounces)

Appendix B: LOS/OLOS RSS versus Distance Data

TABLE B.1: BLE LOS RSS VERSUS DISTANCE

1m	2m	3m	4m	5m
60	69	66	66	66
59	66	70	68	70
63	61	67	62	68
60	63	61	64	63
64	63	63	64	70
67	60	66	60	71
54	60	61	67	66
57	59	63	63	64
52	56	59	61	68
50	55	63	60	66
57	59	57	65	59
56	63	56	63	65
59	65	67	67	64
65	62	69	63	61
63	62	61	63	66
58	64	66	65	66

TABLE B.2: BLE OLOS RSS VERSUS DISTANCE

1m	2m	3m	4m	5m
-75	-82	-81	-80	-87
-73	-81	-80	-79	-88
-74	-80	-79	-81	-85
-75	-79	-80	-81	-84
-76	-80	-79	-81	-86
-75	-82	-78	-83	-85
-72	-81	-79	-82	-84
-74	-80	-80	-79	-83

-74	-80	-79	-81	-85
-75	-80	-78	-80	-84
-74	-81	-80	-79	-85
-73	-80	-79	-80	-84
-76	-79	-80	-81	-83
-75	-78	-79	-80	-85
-74	-81	-78	-80	-84
-73	-82	-79	-81	-85
-72	-80	-80	-82	-86
-74	-79	-81	-81	-87
-75	-80	-79	-80	-86

Appendix C: BLE Path Loss Modelling MATLAB Code

```
clc;close all;clear;

%Parsing measurement data from csv file

data = csvread('no_furniture.csv');

%Distance in meter

d = data(:,1);

%RSS in dB here

Pr = data(:,2);

%Plot your Pathloss versus. Distance

d_dB=10*log10(d);

%Line of Best Fitting

F1=fit(d,Pr,'poly1');

%Plot your data with fitting

plot(F1,d,Pr);

grid on;

title('RSS versus Distance');

xlabel('Distance (m)');

ylabel('RSS[dBm]');

disp(F1);

disp('Mean value of shadow fading is:');

disp(mean(Pr+20+2*d_dB));

disp('Standard Deviation of shadow fading is:');

disp(std(Pr+0+2*d_dB);
```

Appendix D: BLE Ranging Estimation & CRLB Comparison MATLAB Code

```
close all

P_0 = abs(mean(Pr(1:16)));

P_r = Pr*(-1);

alpha = 2.2;

measured_dist = 10.^((abs(P_0 - P_r))/(10*alpha));

actual_dist = d;

figure(1) hold on;grid on;

plot(d,measured_dist,'*');

plot(d,d);

title('BLE Actual Distance versus Measured Distance(m)');

xlabel('Actual Distance');

ylabel('Measured Distance');

figure(5) grid on;hold on;

std_dev1 = sqrt((sum((measured_dist(1:16) - 1).^(2)))/(16-1));

std_dev2 = sqrt((sum((measured_dist(17:32) - 2).^(2)))/(16-1));

std_dev3 = sqrt((sum((measured_dist(33:48) - 3).^(2)))/(16-1));

std_dev4 = sqrt((sum((measured_dist(49:64) - 4).^(2)))/(16-1));

std_dev5 = sqrt((sum((measured_dist(65:80) - 5).^(2)))/(16-1));

std_devall = [std_dev1,std_dev2,std_dev3,std_dev4,std_dev5];

plot([1,2,3,4,5],std_devall,'*');

std_fit = fit([1,2,3,4,5]',std_devall','poly2');

plot(std_fit);

dj = [1,2,3,4,5];

CRLB_OLOS = (((log(10))^2/100).*(dj.^2)*((2.2^2)/(1.6^2)));

CRLB_fit = fit([1,2,3,4,5]',CRLB_OLOS','poly2');

plot(CRLB_fit,'b');

legend('Standard Deviation of Error(m)', 'Stdev Best Fit Curve', 'CRLB Best
Fit Curve');

axis([1 5 0 5]);

title('BLE Standard Deviation of Error versus Distance (CRLB)');

xlabel('Distance(m)');

ylabel('Standard Deviation of Error (m)');
```

Appendix E: UWB Pathloss and TOA Processing MATLAB Code

```
%fname = ['freq1.s1p'];
 tstart=0;
% tstop=300e-9;
tstop = 30e-9;
noi = 10^(-80/20);   %noise threshold
 side =10^(-20/20);
 secPeak=1.62*10^(-9);
 %peak_width = 1/1000;
 peak_width=1;
 flag_fig = 1;
 ampResult = [];
 delayResult = [];
 index = [];
 ftoa=[];
 ftoa_delay=[   ];
 ftoa_amp=[    ];
 TOA_dis=[   ];
 firstPeakDelay = [    ];
 firstPeakAmp = [   ];

 % Rfid = fopen('Result.txt','a');
 bias=0;
 % Read all the data name from filename.txt

for i=7:56

 fname = [num2str(i) '.s1p'];

 [Hf1, f1] = load_chmeas_s1p_dB( fname, flag_fig );
 %[zt_han, t] = czt_hanning( f1, Hf1, tstart, tstop, 1, 1601*1000);
 [zt_han, t] = czt_hanning( f1, Hf1, tstart, tstop, 1, 1601);
```

```
 time_dB = 20*log10(abs(zt_han))-bias;

 % Plot Time Response in Time Domain
 figure(2);hold on;grid on;
 plot(t,time_dB);

 noi = -90;   %noise threshold
 side =-8;

 index = pkd_cir(time_dB, noi, side, peak_width);
%index = pkd_cir(abs(zt_han), noi, side, peak_width);
 if index == 0
     Continue
end
ftoa_delay = [ftoa_delay t(index(1))];
ftoa_amp = [ftoa_amp 20*log10(abs(zt_han(index(1))))-bias];


 figure(4);hold on;grid on;
 title(' First Path Path Loss versus TOA distance');
 xlabel('TOA distance (m)');
 ylabel('Path Loss (dB)');

 figure(2);hold on;grid on;
 xlabel('Delay (s)');
 ylabel('Path Loss (dB)');
 title('Time Domain');

 figure(5);hold on;grid on;
 xlabel('Distance (m)');
 ylabel('TOA Delay (s)');
 title('TOA Delay Versus Distance');
```

```
 figure(6);hold on;grid on;
 xlabel('TOA Delay (s)');
 ylabel('Path loss (dB)');
 title('Path Loss Versus TOA Delay');

plot(t(index(1:length(index))),20*log10(abs(zt_han(index(1:length(index)))))-
bias,'bo');
plot(ftoa_delay,ftoa_amp,'ro');


 ftoa_dist=ftoa_delay*2.99792458*10^8;
 ftoa_dist_real= linspace(.1,5,50);
 TOA_dis=[TOA_dis,ftoa_dist];


 figure(4);hold on;
 plot(ftoa_dist,ftoa_amp,'*');


 figure(5);hold on;
 plot(ftoa_dist,ftoa_delay,'*');


 figure(6);hold on;
 plot(ftoa_delay,ftoa_amp,'ro');


 figure(7);hold on; grid on;
 plot(ftoa_dist_real,ftoa_delay,'*');
 title("Actual Distance versus FTOA Delay");
 xlabel("Distance (m)");
 ylabel("Delay (s)");


End
```

Appendix F: UWB Shadow Fading Functions

```
clear all
close all
clc
%fname = ['freq1.s1p'];
tstart=0;
% tstop=300e-9;
tstop = 30e-9;
noi = 10^(-80/20);   %noise threshold
side =10^(-20/20);
secPeak=1.62*10^(-9);
%peak_width = 1/1000;
peak_width=1;
flag_fig = 1;
ampResult = [];
delayResult = [];
index = [];
ftoa=[];
ftoa_delay=[   ];
ftoa_amp=[    ];

TOA_dis=[   ];

firstPeakDelay = [    ];
firstPeakAmp = [   ];

%  Rfid = fopen('Result.txt','a');

bias=0;
% Read all the data name from filename.txt

figure(4);hold on;grid on;
title('Path Loss versus Estimated distance');
```

```
xlabel('Estimated Distance (m)');
ylabel('Path Loss (dB)');

figure(2);hold on;grid on;
xlabel('Delay (s)');
ylabel('Path Loss (dB)');
title('Path Loss versus TOA');

% figure(5);hold on;grid on;
% xlabel('Distance (m)');
% ylabel('TOA Delay (s)');
% title('TOA Delay Versus Distance');

%figure(6);hold on;grid on;
%xlabel('TOA Delay (s)');
%ylabel('Path loss (dB)');
%title('Path Loss Versus TOA Delay');

for i = 1

%     if i ~= 9
        fname = [num2str(i) '.s1p'];

        [Hf1, f1] = load_chmeas_s1p_dB( fname, flag_fig );
        %[zt_han, t] = czt_hanning( f1, Hf1, tstart, tstop, 1, 1601*1000);
        [zt_han, t] = czt_hanning( f1, Hf1, tstart, tstop, 1, 1601);

        time_dB = 20*log10(abs(zt_han))-bias;
%         figure(1);hold on;grid on;
%         plot(t,abs(zt_han));
        % Plot Time Response in Time Domain
        figure(2);hold on;grid on;
        plot(t,time_dB);
```

```
        noi = -89.5;    %noise threshold

        side =-13;

        index = pkd_cir(time_dB, noi, side, peak_width);

        %  index = pkd_cir(abs(zt_han), noi, side, peak_width);
        if index == 0
            continue
        end

        ftoa_delay = [ftoa_delay t(index(1))];
        ftoa_amp = [ftoa_amp 20*log10(abs(zt_han(index(1))))-bias];



        figure(2);hold on;
plot(t(index(1:length(index))),20*log10(abs(zt_han(index(1:length(index)))))-
bias,'bo');
        plot(ftoa_delay,ftoa_amp,'ro');



        ftoa_dist=ftoa_delay*2.99792458*10^8;
%         ftoa_dist_real= linspace(.1,5,50);
        %error = abs(subtract(ftoa_dist_real,ftoa_dist));
        d1 = [1,1,1,1,1,1,1,1];
        d2 = 2*d1;
        d3 = 3*d1;
        d4 = 4*d1;
        d5 = [5,5,5,5,5,5,5];
        ftoa_dist_real= [d1,d2,d3,d4,d5];
        TOA_dis=[TOA_dis,ftoa_dist];
```

```
        figure(4);hold on;
        plot(ftoa_dist,ftoa_amp,'*');
        title('Path Loss versus TOA distance');
        xlabel('TOA distance (m)');
        ylabel('Path Loss (dB)');
        figure(5);hold on;
        plot(ftoa_dist,ftoa_delay,'*');

        figure(6);hold on;
        plot(ftoa_delay,ftoa_amp,'ro');
%     end

end
% ftoa_dist_store = ftoa_dist;
% figure(3); hold on; grid on;
diff_x = ftoa_dist - ftoa_dist_real;
error = diff_x;
figure(7);hold on; grid on;
plot(ftoa_dist_real, ftoa_dist, '*');
hold on;
% jx = fit (ftoa_dist_real',ftoa_dist','poly1');
% plot(jx);
% ylim([0 7]);
x = ftoa_dist_real;
y = x + 0.1931;

% plot(ftoa_dist_real,ftoa_delay,'*');
title("UWB Estimated versus Actual Distance");
xlabel("Actual Distance (m)");
ylabel("TOA Distance (m)");
line(x,y,'Color', 'Red');
line(x,x, 'Color','Blue');
legend('Estimated Distance Points','Average', 'Ideal');
```

```
sq_x = diff_x .* diff_x;
thehnumbah = mean(sq_x);
average_error = mean(error(1:39));
figure(8);hold on; grid on;
plot(ftoa_dist_real,error,'*');
axis([1 5 -1 1]);
title("UWB Error versus Distance");
% axis([0 5 -2 1]);
% FX = fit(ftoa_dist_real',error','poly1');
% plot(FX);

% ylim([0 2]);
% d = ftoa_dist_real;%[1,2,3,4,5];
% CRLB_OLOS = (((log(10))^2/100).*(d.^2)*((7.9766^2)/(3.994^2)));
% CRLB_LOS = (((log(10))^2/100).*(d.^2)*((5.2709^2)/(3.043^2)));

% STD_ER_OLOS = sqrt(CRLB_OLOS);
% STD_ER_LOS = sqrt (CRLB_LOS);
% plot();
xlabel('Distance (m)');
ylabel('Error (m)');
% % % % % % % % % % % % %
mean_1m = mean(error(1:8));
mean_2m = mean(error(9:16));
mean_3m = mean(error(17:24));
mean_4m = mean(error(25:32));
mean_5m = mean(error(33:39));
mean_all_dist = [mean_1m,mean_2m,mean_3m,mean_4m,mean_5m];
d_vec = [1,2,3,4,5];

% figure(9);hold on;grid on;
% plot(d_vec,mean_all_dist,'*');
```

```
% hold on;
% err_fit = fit(d_vec',mean_all_dist','poly1');
% plot(err_fit);
% title('Average Error at actual distance');
% xlabel('Distance (m)');
% ylabel('Average Error (m)');

% % % % % % % % % % % % % % %
% var_1m = var(ftoa_dist(1:8));
% var_2m = var(ftoa_dist(9:16));
% var_3m = var(ftoa_dist(17:24));
% var_4m = var(ftoa_dist(25:32));
% var_5m = var(ftoa_dist(33:39));

% sd_1m = std(error(1:8));
% sd_2m = std(error(9:16));
% sd_3m = std(error(17:24));
% sd_4m = std(error(25:32));
% sd_5m = std(error(33:39));
% sd_all_dist = [sd_1m,sd_2m,sd_3m,sd_4m,sd_5m];

% figure(10);hold on;grid on;
% plot(d_vec,sd_all_dist,'*');
% hold on;
% var_fit = fit(d_vec',sd_all_dist','poly1');
% plot(var_fit);
% hold on;
% axis([1 5 0 4]);
% title('Standard Deviation at actual distance');
% xlabel('Distance (m)');
% ylabel('Standard deviation (m)');

figure(11);hold on;
```

```
std_dev_1 = sqrt((sum((ftoa_dist(1:8)-1).^(2)))/(8-1));
std_dev_2 = sqrt((sum((ftoa_dist(9:16)-2).^(2)))/(8-1));
std_dev_3 = sqrt((sum((ftoa_dist(17:24)-3).^(2)))/(8-1));
std_dev_4 = sqrt((sum((ftoa_dist(25:32)-4).^(2)))/(8-1));
std_dev_5 = sqrt((sum((ftoa_dist(33:39)-5).^(2)))/(7-1));
std_dev_all = [std_dev_1, std_dev_2, std_dev_3, std_dev_4, std_dev_5];
plot([1,2,3,4,5], std_dev_all, '*');
grid on;
hold on;
std_dev1= mean(std_dev_all);
std_mat = std(error(1:39));
std_dev = sqrt((sum((ftoa_dist(1:39)-ftoa_dist_real(1:39)).^(2)))/(39-1));
var = std_dev^2;
var1 = std_dev1^2;
% figure(13); hold on; grid on;
% plot(ftoa_dist_real,std_dev);
% hold on;
line([0,5],[0.033,0.033]);
% line([0,5],[var,var]);
% axis([0 5 0 0.07]);

std_fit = fit(d_vec',std_dev_all','poly1');
plot(std_fit);
axis([0 5 0 3]);
title('UWB Standard Deviation versus Distance (CRLB)');
xlabel('Distance (m)');
ylabel('Standard deviation (m)');
legend('Standard deviation (at each meter)','CRLB Line', 'Var Line');

figure(12);hold on;
% histogram(error(1:50));
% rng default;
```

```
histfit(error(1:39));
%
title('UWB Histogram of Error');
xlabel('Error (m)');
ylabel('Quantity of Error');
% pd = fitdist(r, 'Normal');
% figure(9);hold on; grid on;
%figure(11);hold on;grid on;
%histogram(error,10);
% plot(d,STD_ER_LOS);
% title('Standard Deviation of Error versus Distance (LOS)');
% xlabel('Distance');
% ylabel('Standard Deviation of Error');
figure(88);hold on;grid on;
plot(ftoa_dist(1:8),ftoa_amp(1:8),'r*');
plot(ftoa_dist(9:16),ftoa_amp(9:16),'g*');
plot(ftoa_dist(17:24),ftoa_amp(17:24),'b*');
plot(ftoa_dist(25:32),ftoa_amp(25:32),'k*');
plot(ftoa_dist(33:39),ftoa_amp(33:39),'m*');
title('Path Loss versus TOA distance');
xlabel('TOA distance (m)');
ylabel('Path Loss (dB)');
legend('1m','2m','3m','4m','5m');
```

Appendix G: UWB MATLAB Code Helper Functions

Peak detection:

```
%
% Peak detection on channel impulse response.
%
% input:
%       ht: channel impulse response
%       noi: threshold for noise std
%       side: sidelobe amplitude for window functions
%           Rec: -13dB, Hanning: -32dB, Hamming: -43dB
%       peak_width: time resolution of peak in units of dt

function [ peak_index ] = pkd_cir(ht, noi, side, peak_width)
% peak_width is not used in this version.
len_t = length(ht);
peak = max(ht);
peak_index = 0;
count = 0;
i = 2;
while(1)
    %%%%%%%%%%%%%Orignal(mw)%%%%%%%%%%%%%%%%%%%%%
%     if ht(i)>ht(i-1) & ht(i)>ht(i+1) & ht(i)>noi & ht(i)/peak > side
    %%%%%%%%%%%%%Orignal%%%%%%%%%%%%%%%%%%%%%%%
     %%%%%%%%%%%%%Jie He(db)%%%%%%%%%%%%%%%%%%%%%
    if ht(i)>ht(i-1) & ht(i)>ht(i+1) & ht(i)>noi & ht(i)-peak > side
         %%%%%%%%%%%%%Jie He%%%%%%%%%%%%%%%%%%%%%%


        if count == 0
            peak_index = i;
            count = 1;
        else
```

```
            peak_index = [peak_index, i];
        end;
        i = i + 1;
    else
        i = i + 1;
    end;

    if i > len_t - 1
        break;
    end;
end;
return;
```

Vector Network Analyzer Data Processing:

```
%
% This program is used to load 8753D Network Analyzer Measurement data.
% Read S21 data from S1P file.  LogMag/Angle.
%

function [ Hf, f ] = load_chmeas_s1p_dB( fname, flag_fig)

%fid = fopen(fname, 'rt');
fid = fopen(fname, 'rt');
if fid == -1
    disp(['File cannot be opened !']);
    Hf = 0;  f = 0;
    return;
end;
```

```
while( 1 )
    temp_str = fgetl(fid);  % read in a line of text.

    if temp_str(1) == '!'
        if flag_fig == 1
            disp(temp_str);
        end;
    else
        if temp_str(1) == '#'
            tmp_data = fscanf(fid, '%g %g %g', [3 inf] );
            fclose(fid);

            tmp_data = tmp_data.';
            f = tmp_data(:,1);
            amp = 10.^(tmp_data(:,2)/20);
      % Channel Transfer Function measured by VNA
            %      Hf = 10.^(tmp_data(:,2)/20).*exp(1j*tmp_data(:,3)*pi/180);
            Hf = amp.*exp(1j*tmp_data(:,3)*pi/180);
            break;
        else
            if feof(fid)
                fclose(fid);
                Hf = 0;  f = 0;
                return;
            end;
        end;
    end;
end;



% %Plot figure in frequency domain - disable while looping
% if flag_fig == 1
```

```
%     tmp_f = f*1e-9;
%     mag_dB = 10*log10(abs(Hf));
%     phs = angle(Hf.');
%
%     figure; hold on; box on;
%    subplot(2,1,1);  plot(tmp_f, mag_dB);
%     subplot(2,1,1);  plot(tmp_f, mag_dB);
%     xlabel('frequency (GHz)');
%     ylabel('Magnitude (dB)');
%     title(fname);
%
%     subplot(2,1,2);  plot(tmp_f, phs);
%     xlabel('frequency (GHz)');
%     ylabel('angle (radian)');
% end;

return;
```

Channel Impulse Response Calculation:

```
% Compute Channel Impulse Response from frequency measurement
% data using Chirp-Z transform with hanning window.
% modified 03/27/02.

function [ zt_han , t ] = czt_hanning(freq, Zf, tstart, tstop, flag, Nt )

%Nf = length(freq);
Nf = length(freq);
df = (freq(Nf)-freq(1))/(Nf-1);

T = 1/df;
```

```
if nargin < 6
 % Nt = 1601;
  Nt = 1601;
end;


if flag == 1
  han = hanning(Nf);
%  han = hann(Nt);
  Zf = (45/23)*Zf(:).*han(:);  % 45/23 is to make the Hanning-window time
response peak at 1.
%   Zf = Zf(:).*han(:);
end;


dt = (tstop-tstart)/(Nt-1);
w = exp(1j*2*pi*dt/T);
a = exp(1j*2*pi*tstart/T);


zt_han = (1/Nf)*czt(Zf(:), Nt, w, a);


t = linspace(tstart, tstop, Nt);


return;
```

References

Apsima. (Sep 12, 2014). *iBeacons for Logistics: A Use Case in Facilities, Asset, and Inventory Management.* Apsima blog. Retrieved from: http://apsima.com/blog/ibeacon-for-logistics-facilities-asset-inventory-management/

CGI. (n.d.) *Digital Solutions for Strengthening Customer Focus and Achieving Cost Savings.* Retrieved from: https://admin.cgi.com/en/post-and-logistics

Chen, W. Hansenfield, E. Loftin, S. St. Pierre, S. (March, 2017). *Indoor Localization via Maximum Likelihood using Low-Energy Bluetooth iBeacon Technology.* Worcester Polytechnic Institute.

Connor, J. C. Goodrich, D. J. Alhumoud, Q. A. (2017). *Using iBeacon for Navigation and Proximity Awareness in Smart Buildings.* Worcester Polytechnic Institute. Retrieved from: https://digitalcommons.wpi.edu/cgi/viewcontent.cgi?article=1842&context=mqp-all

Elgan, Mike. (Sep 14, 2013). *Why Apple's 'indoor GPS' plan is brilliant.* IDG Communications. Retrieved from: https://www.computerworld.com/article/2485049/mobile-payments/why-apple-s--indoor-gps--plan-is-brilliant.html

Estimote, Inc. (2017). *Beacons, how do they work?* Estimote Developer Docs. Retrieved from: https://developer.estimote.com/how-beacons-work/

Estimote, Inc. (2017). *Technical Specification of Estimote Beacons and Stickers.* Retrieved from: https://community.estimote.com/hc/en-us/articles/204092986-Technical-specification-of-Estimote-Beacons-and-Stickers

iBeacon Insider. (n.d.). *What is iBeacon? What are iBeacons?* iBeacon Guide. Retrieved from: http://www.ibeacon.com/what-is-ibeacon-a-guide-to-beacons/

Laney, Brian. (July 1, 2015). *5 Companies using iBeacon Technology to Make More Money*. Alert Tech. Retrieved from: http://alerttech.net/5-companies-using-ibeacon-technology-earn-money/

Locatify. (June 15, 2017). *iBeacons or UWB for Indoor Proximity Services.* Locatify. Retrieved from: https://locatify.com/blog/ble-beacons-versus-UWB-for-indoor-gps-proximity-rtls/

MDPI. (July 16, 2016). *Ultra Wideband Indoor Positioning Technologies: Analysis and Recent Advances.* Retrieved October 11, 2018, from: res.mdpi.com/sensors/sensors-16-00707/article_deploy/sensors-16-00707-v2.pdf?filename=&attachment=1

Muller, J. (n.d.). *GPS for Today*. Retrieved from: http://www.gpsfortoday.com/about/

Pahlavan, K. Krishnamurthy, P. (Jan, 2013). *Principles of Wireless Access and Localization.* West Sussex, United Kingdom: John Wiley & Sons Ltd.

Pahlavan, K. (Feb 22, 2019). *Indoor* Geolocation *Science and Technology: At the Emergence of Smart World and IoT*. River Publishers.

Persistence Market Research. (Oct 30, 2017). *Bluetooth Beacon and iBeacon market is expected to grow at a CAGR of 91.4% by 2025.* Retrieved from: https://globenewswire.com/news-release/2017/10/30/1159903/0/en/Bluetooth-Beacon-and-iBeacon-Market-is-projected-to-grow-at-a-CAGR-of-91-4-by-2025-Persistence-Market-Research.html

Robin HelpCenter. (2017). *Where to place beacons for the best coverage.* Robin Powered, Inc. Retrieved from: https://support.robinpowered.com/hc/en-us/articles/204278994-Where-to-place-beacons-for-the-best-coverage

Shrestha, B. (Oct 6, 2016). *Measurement of Power Consumption of BLE (Bluetooth Low Energy).* Helsinki Metropolia University of Applied Sciences. Retrieved from: https://www.theseus.fi/bitstream/handle/10024/118662/Shrestha_Bikash.pdf?sequence=1